Inorganic Chemistry

Article

Cite This: Inorg. Chem. XXXX, XXX, XXX-XXX

pubs.acs.org/IC

Construction of Novel Cyclic Tetrads by Axial Coordination of Thiaporphyrins to Tin(IV) Porphyrin

A. Alka,[†,‡] Yogita Pareek,[†,‡] Vijayendra S. Shetti,[†] M. Rajeswara Rao,[†] Gregory G. Theophall,[§] Way-Zen Lee,[⊥] K. V. Lakshmi,*[,§] and M. Ravikanth*[,†]

[†]Department of Chemistry, Indian Institute of Technology Bombay, Powai, Mumbai 400 076, India

[§]Department of Chemistry and Chemical Biology and The Baruch '60 Center for Biochemical Solar Energy Research, Rensselaer Polytechnic Institute, Troy, New York 12180, United States

[⊥]Instrumentation Center, Department of Chemistry, National Taiwan Normal University, 88 Section, 4 Ting-Chow Road, Taipei 11677, Taiwan

Supporting Information

ABSTRACT: We report the formation of new cyclic porphyrin tetrads **1** and **2**, which were obtained from the reaction between dihydroxytin(IV) porphyrin and *cis*-dihydroxy-21-thiaporphyrin/21,23-dithiaporphyrin. The unique oxophilicity of tin(IV) porphyrin was the driving force for the formation of these tetrads. Moreover, these novel tetrads represent the first examples of cyclic porphyrins containing tin(IV) that are constructed exclusively on the basis of the "Sn−O" interaction without any other complementary, noncompetitive mode of interactions. The molecular structures of the cyclic tetrads have been investigated by matrix-assisted laser desorption ionization time-of-flight mass spectrometry, NMR spectroscopy, quantum-mechanical calculations, and, in one case, single-crystal X-ray crystallography. The X-ray structure revealed that the two *cis*-dihydroxy-N_2S_2 porphyrins were coordinated at the axial positions of two tin(IV) porphyrins, leading to the symmetric cyclic tetrad structure. The optical properties of tetrads were studied, and these compounds were stable under redox conditions. Preliminary photophysical studies carried out on the tetrads indicated efficient energy transfer from tin(IV) porphyrin to the thiaporphyrin unit, which highlights their potential applications in energy and electron transfer in the future.

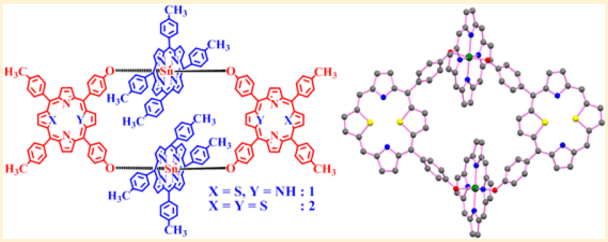

INTRODUCTION

Synthetic multiporphyrin arrays have often been used in optoelectronic devices and have also served as structural and functional models to understand energy- and electron-transfer processes in nature.[1−14] Both covalent and noncovalent approaches have been used for the construction of multiporphyrin arrays. There are certain limitations associated with the covalent strategies that have been employed previously, such as the need for multistep reactions and separation of the resulting statistical mixture of products that often involves tedious column chromatographic purifications and low product yields. These limitations can be overcome by the use of noncovalent strategies that lead to the easier isolation of products with higher yields.[15−19] In previous studies, coordination, multiple hydrogen bonds, or a combination of the two have been widely used as the source of noncovalent interactions.[5,20−22] An "axial-bonding" approach has also be used to create "donor−acceptor" multiporphyrin arrays, where porphyrins with a peripheral functional group are coordinated to the metal center of a metalloporphyrin.[9] In this case, the porphyrins or metalloporphyrins serve as suitable building blocks if they contain donor groups such as pyridyl, imidazole, aryloxide, and carboxyaryl moieties at peripheral position(s) that are capable of coordinating to the metal center of a metalloporphyrin.[21,22] In turn, metalloporphyrins can act as acceptors if they have vacant axial coordination site(s) on the metal center. It is well documented in the literature that porphyrins containing N-donor ligands such as pyridyl, imidazole, pyrazole, or amine functional groups prefer coordinating to metalloporphyrins with a Zn^{II}, Ru^{II}, Os^{II}, Rh^{II}, Pt^{II}, or Pd^{II} center.[5,23−27] In contrast, porphyrins with O-donor ligands such as carboxylate or aryloxide groups prefer coordinating to Fe^{III}-, Mn^{III}-, Al^{III}- or Sn^{IV}-containing metalloporphyrins to form axial multiporphyrin arrays. Multiporphyrin arrays based on metal−N interactions have been extensively investigated in the literature.[5,16,28] However, multiporphyrin arrays containing metal−O interactions are rather limited.[24,25,29−33]

Tin(IV) porphyrins belong to a class of oxophilic metalloporphyrins[34−41] that are ideal building blocks for the construction of multiporphyrin assemblies for the following reasons:[42,43] (a) Tin(IV) porphyrins are stable in both acidic and basic environments. (b) They are diamagnetic, which

Received: August 7, 2017

DOI: 10.1021/acs.inorgchem.7b01966
Inorg. Chem. XXXX, XXX, XXX−XXX

Chart 1. Molecular Structures of Acyclic Arrays That Are Based on Tin(IV) Porphyrin Involving Noncompetitive Interactions

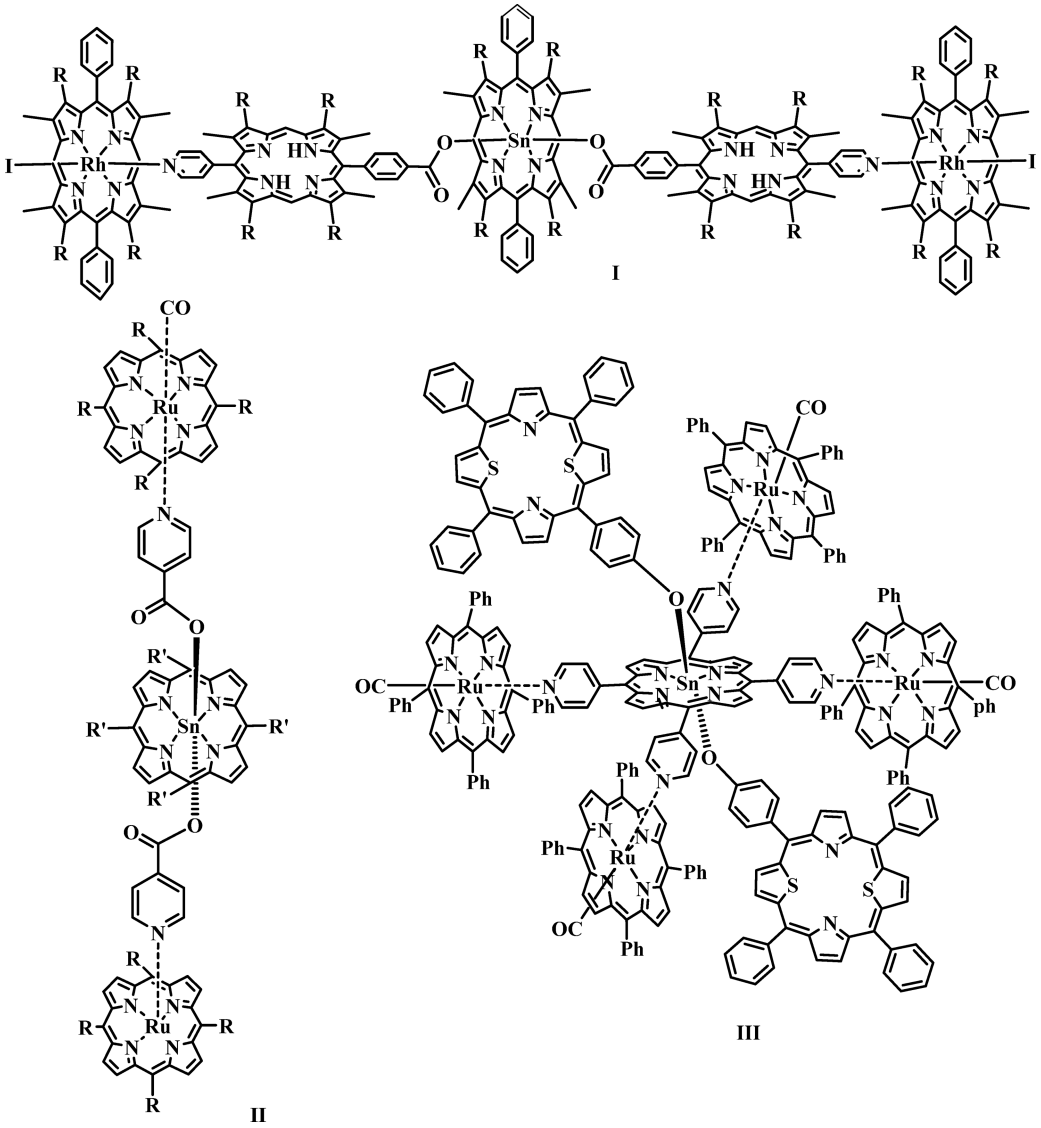

Chart 2. Molecular Structures of Cyclic Arrays That Are Based on Tin(IV) Porphyrin Involving Complementary Interactions

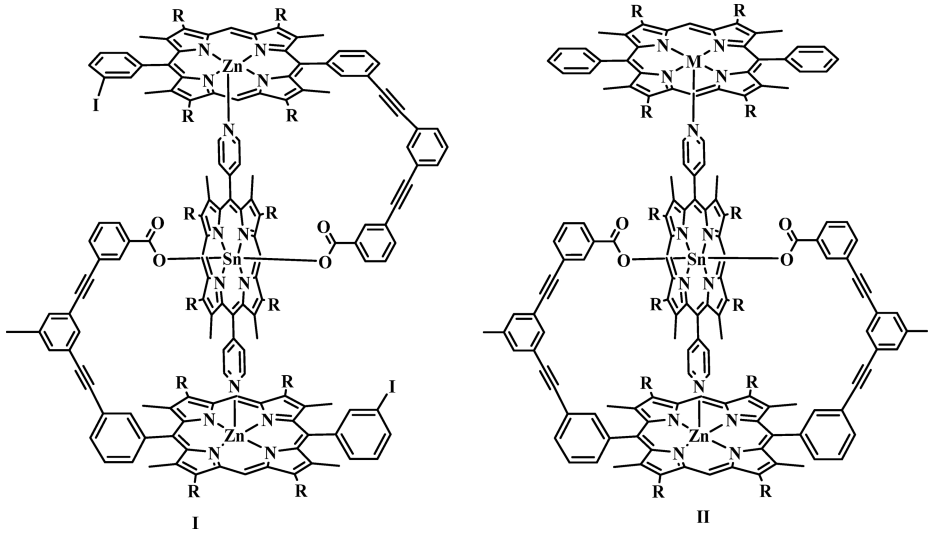

DOI: 10.1021/acs.inorgchem.7b01966
Inorg. Chem. XXXX, XXX, XXX−XXX

Chart 3. Molecular Structures of Cyclic Tetrads 1 and 2 That Were Synthesized in This Study

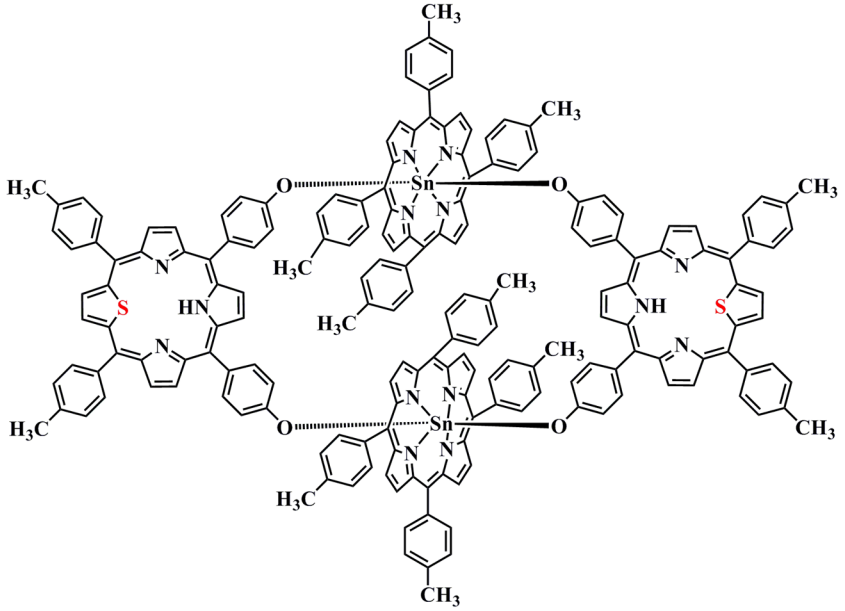

Tetrad **1**

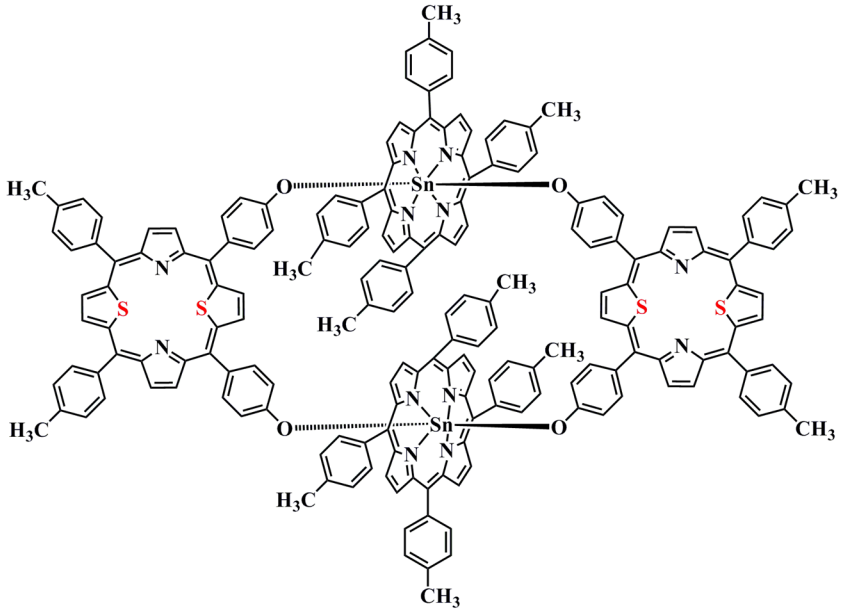

Tetrad **2**

makes them highly suitable for structure determination by NMR spectroscopy; moreover, Sn is an NMR-active nucleus that can be used as a structural probe. (c) The optical properties of tin(IV) porphyrins are attractive, and these complexes are also luminescent. (d) Tin(IV) porphyrins are easier to reduce in comparison with other diamagnetic metalloporphyrins. (e) Tin(IV) porphyrins exhibit coordination specificity toward O-donor ligands. Sanders and other researchers have previously demonstrated the construction of elegant tin(IV) porphyrins that were based on the supramolecular structures shown in Chart 1.[6,23,25,44−47] Interestingly, supramolecular systems based on tin(IV) porphyrins in the literature have always been constructed using porphyrins with a single O-donor group such as a phenoxy or an arylcarboxy group.[7,9,23,25,30,31,48] Moreover, tin(IV) porphyrin based cyclic porphyrin arrays have been constructed with "Sn−O" and other complementary, noncompetitive metal−ligand interactions, such as, "Ru−N or Zn−N" interactions (Chart 2).[44,48] However, to the best of our knowledge, tin(IV) porphyrin based cyclic multiporphyrin arrays with porphyrins containing two O-donor groups that are based exclusively on "Sn−O" interactions have not been reported in the literature thus far.[48] Here, we report the first examples of cyclic porphyrin tetrads **1** and **2** (Chart 3), which were constructed by a reaction between dihydroxytin(IV) porphyrins and *cis*-dihydroxyphenyl thiaporphyrins, exclusively involving "Sn−O" interactions as a driving

DOI: 10.1021/acs.inorgchem.7b01966
Inorg. Chem. XXXX, XXX, XXX−XXX

Scheme 1. Synthesis of the Monomeric Building Blocks 3 and 4

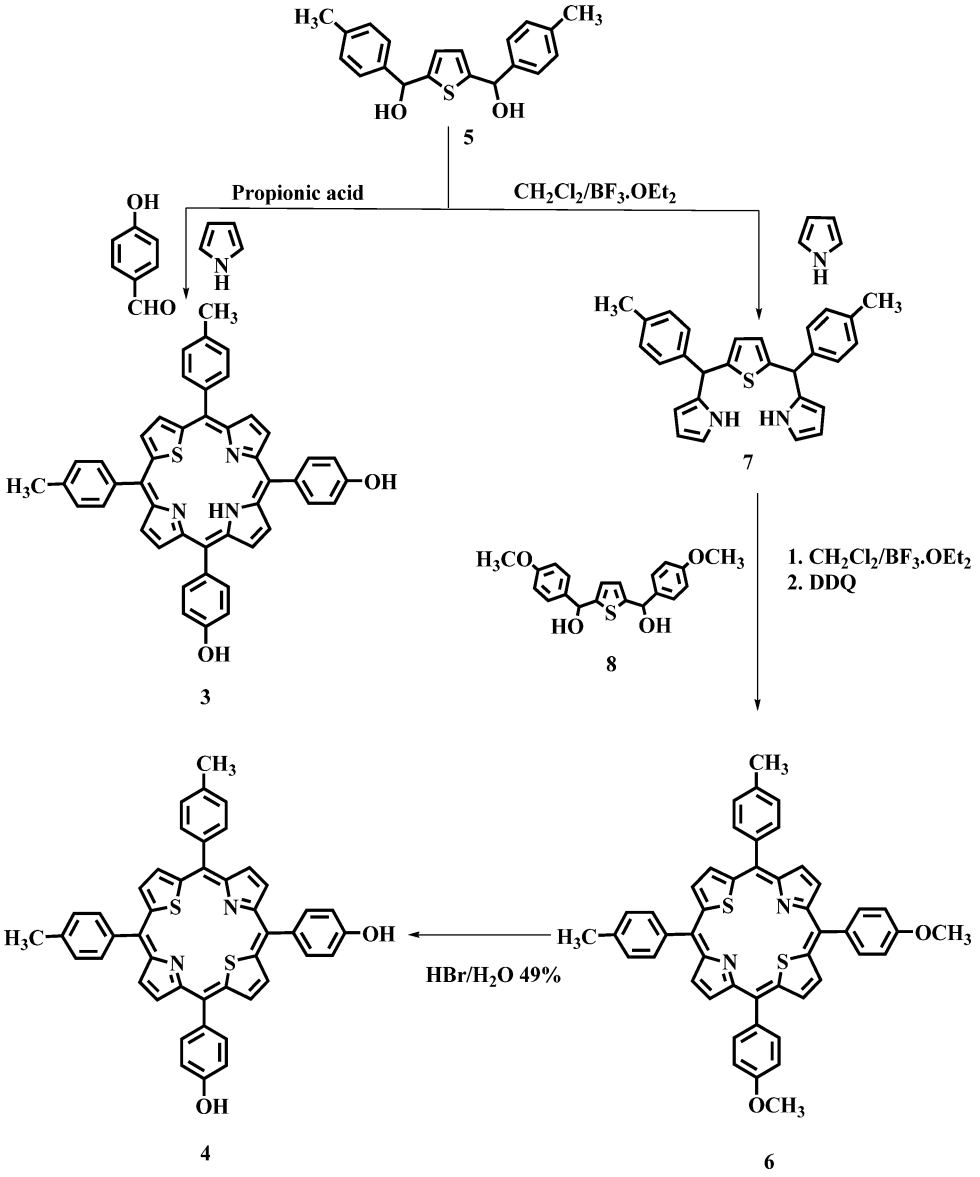

force. These cyclic tetrads are robust to column chromatographic purification and have been characterized by mass spectrometry (MS), 1D and 2D NMR, absorption, and fluorescence spectroscopy, and electrochemical and quantum-mechanical studies. In particular, the single-crystal X-ray crystallography, quantum-mechanical density functional theory (DFT), and time-dependent DFT (TD-DFT) studies were used to understand the geometric structure and optical properties of the cyclic tetrads. The photophysical studies supported the possibility of energy transfer from tin(IV) porphyrin to N_2S_2 porphyrin, which, in turn, indicates their potential applications in energy- and electron-transfer reactions.

RESULTS AND DISCUSSION

Preparation of the Cyclic Arrays. The desired key building blocks *cis*-dihydroxyphenyl monothiaporphyrin **3** (N_3S core) and *cis*-dihydroxyphenyl dithiaporphyrin **4** (N_2S_2 core) for construction of the cyclic tetrads were synthesized according to Scheme 1. Condensation of 2,5-bis(*p*-tolylhydroxylmethyl)thiophene (thiophene diol) **5** (1 equiv) with 4-hydroxybenzaldehyde (2 equiv) and pyrrole (3 equiv) in propionic acid at reflux conditions followed by silica gel column chromatographic purification yielded compound **3** in 10% yield. The second building block, *cis*-dihydroxyphenyl-21,23-dithiaporphyrin **4**, was synthesized in two steps. In principle, condensation of 16-thiatripyrrane with 2,5-bis(4-hydroxyphenyl)hydroxymethylthiophene should yield **4**. However, the difficulty involved in the synthesis of 2,5-bis(4-hydroxyphenyl)hydroxymethylthiophene prompted us to devise a two-step synthesis for **4**. First, the building block *cis*-dimethoxyphenyl-21,23-dithiaporphyrin **6** was synthesized by the Lewis acid catalyzed condensation of 16-thiatripyrrane and 2,5-bis(*p*-anisyl)hydroxymethylthiophene **8** followed by 2,3-dichloro-5,6-dicyanobenzoquinone (DDQ) oxidation in dichloromethane. In the next step, porphyrin **6** was refluxed with 49% hydrogen bromide/water to obtain **4** in good yield. The dihydroxytin(IV) porphyrin building block **9** [SnTPP-$(OH)_2$] was synthesized by following a method previously reported by us.[49] The building blocks **3**, **4**, and **9** were fully characterized by MS and NMR and absorption spectroscopy.

DOI: 10.1021/acs.inorgchem.7b01966
Inorg. Chem. XXXX, XXX, XXX−XXX

Scheme 2. Synthesis of Cyclic Arrays 1 and 2 That Are Based on Tin(IV) Porphyrin

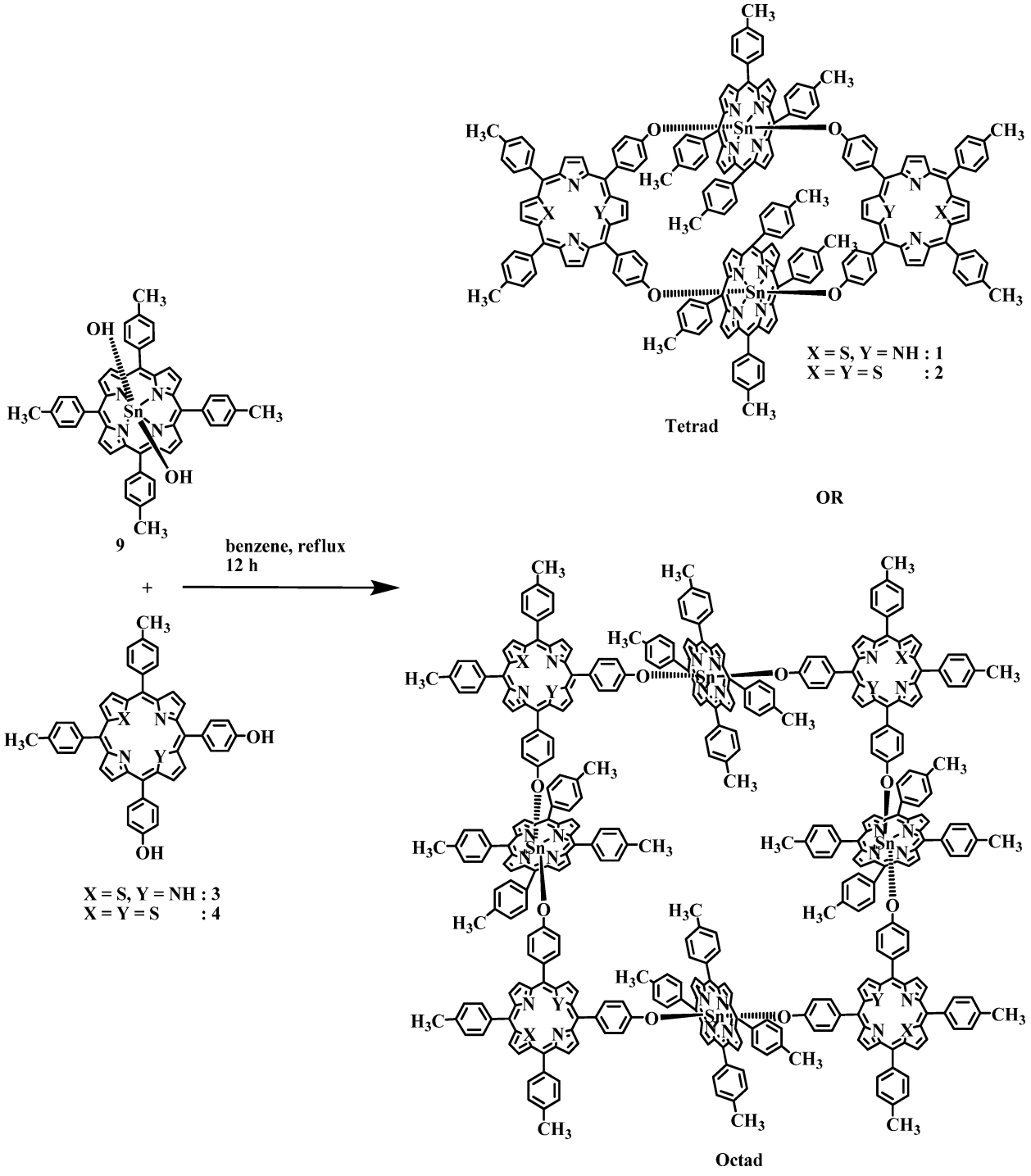

The cyclic arrays, **1** and **2**, were synthesized as depicted in Scheme 2. The reaction was carried out by refluxing **9** (1 equiv) with **3**/**4** (1 equiv) in benzene for a period of 12 h. The progress of the reaction was followed by thin-layer chromatography (TLC) analysis and absorption spectroscopy. The UV–vis spectrum of an aliquot of the reaction mixture displayed broad absorption bands that were bathochromically shifted in comparison with a 1:1 mixture of monomers, indicating formation of the product. Similar TLC and absorption spectral patterns were observed when 2 equiv of **3** or **4** were used in the reaction. This indicated that changing the ratio of the monomers from 1:1 to 1:2 in the reaction did not affect the formation of the final product. As shown in Scheme 2, the reaction between **9** and **3** or **4** can yield two different types of cyclic porphyrin arrays, namely, either a tetrad (**1** or **2**) or an octad. The first evidence in favor of tetrad formation was the presence of a molecular ion peak at 2956.7 corresponding to the molecular structure of tetrad **1** in the matrix-assisted laser desorption ionization time-of-flight (MALDI-TOF) MS spectrum of **1** (Figure S8). A detailed analysis of the NMR spectra will be presented later because the ^{1}H NMR spectrum for both the octad and tetrad is expected to be similar in terms of proton integration ratios. To further strengthen the observation of a tetrad in the MALDI-TOF MS spectrum, we performed DOSY

DOI: 10.1021/acs.inorgchem.7b01966
Inorg. Chem. XXXX, XXX, XXX−XXX

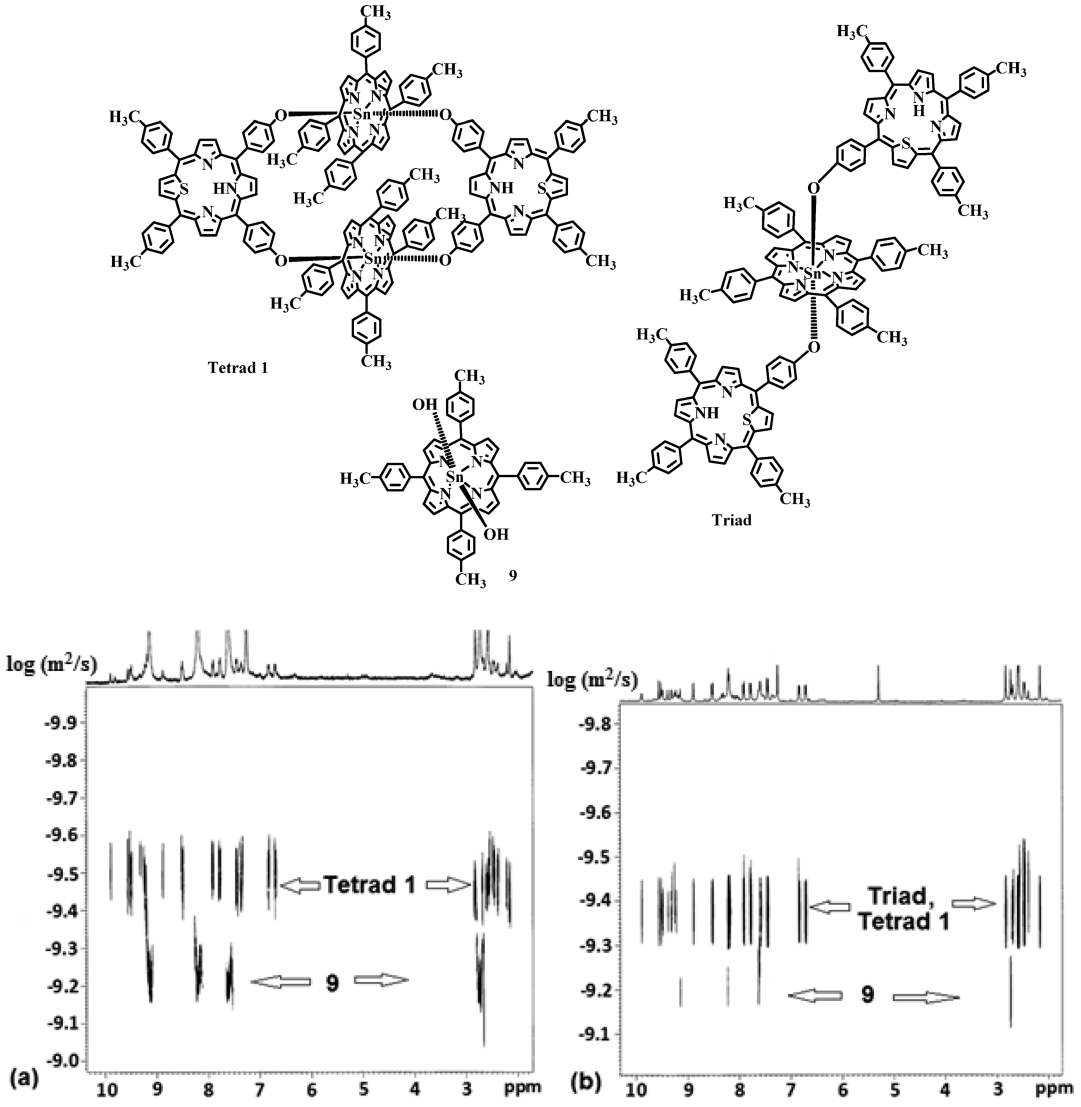

Figure 1. DOSY NMR spectra of (a) a mixture of tetrad **1** and $SnTTP(OH)_2$ **9** and (b) a mixture of triad, tetrad **1**, and $SnTTP(OH)_2$ **9**.

NMR spectroscopy and computationally estimated the thermodynamics of cyclic array formation and X-ray crystallography.

DOSY NMR Spectroscopy of the Cyclic Arrays. We performed DOSY NMR spectroscopy to understand the nature of the cyclic arrays that were formed in the reaction because it provides a direct measure of the diffusion coefficients of molecules in solution. Moreover, the diffusion coefficients depend on the size and shape of the molecules, which makes it possible to distinguish between the formation of tetrads or octads in the reaction. The DOSY experiments revealed that the diffusion coefficients of the cyclic array **1** and tin(IV) porphyrin monomer **9** were 3.63×10^{-10} and 5.37×10^{-10} m^2 s^{-1}, respectively. These coefficients suggest that monomer **9**, which is smaller in size, diffuses faster than the cyclic array **1**. Further, DOSY spectroscopy of a mixture containing the tin(IV) porphyrin monomer **9**, a linear triad,[33] and the cyclic array **1** (Figure 1) indicated that the triad and cyclic array exhibited similar diffusion coefficients. Because the diffusion coefficients did not vary significantly from the triad to the cyclic array under examination, this suggests that the compound with a diffusion coefficient of 3.63×10^{-10} m^2 s^{-1} represents a cyclic tetrad and not an octad.

Thermodynamic Investigations of Cyclic Array Formation. We performed computational studies in order to identify the thermodynamically preferred pathway for the formation of cyclic arrays, namely, tetrads and octads (Schemes S1−S3 and Figures S4−S6). We conceived the structures of the tetrad, octad, and all of the intermediates starting from the monomeric unit (Figure 2), and the structures were optimized and characterized as minima on a potential energy surface. Initially, the probable pathways for the formation of a tetrad and an octad were analyzed by considering the stoichiometric equation that includes the reactants, dihydroxytin(IV) porphyrin (**SP**) and *cis*-dihydroxythiaporphyrin (**TP**), and products (tetrad and octad). The equations with the estimated reaction energies that were obtained for the formation of the tetrad and octad are shown in eqs 1 and 2, respectively:

$$4\,SP + 4\,TP \xrightarrow{-8H_2O} 2\,Tetrad\ (\Delta E = -79.1\ kcal/mol) \quad \ldots\ eq.\ 1$$

$$4\,SP + 4\,TP \xrightarrow{-8H_2O} Octad\ (\Delta E = -48.2\ kcal/mol) \quad \ldots\ eq.\ 2$$

The estimated reaction energies for the formation of the tetrad and octad obtained from the computational studies were −79.1 and −48.2 kcal mol^{-1}, respectively, which revealed that the formation of the tetrad is thermodynamically preferred over

DOI: 10.1021/acs.inorgchem.7b01966
Inorg. Chem. XXXX, XXX, XXX−XXX

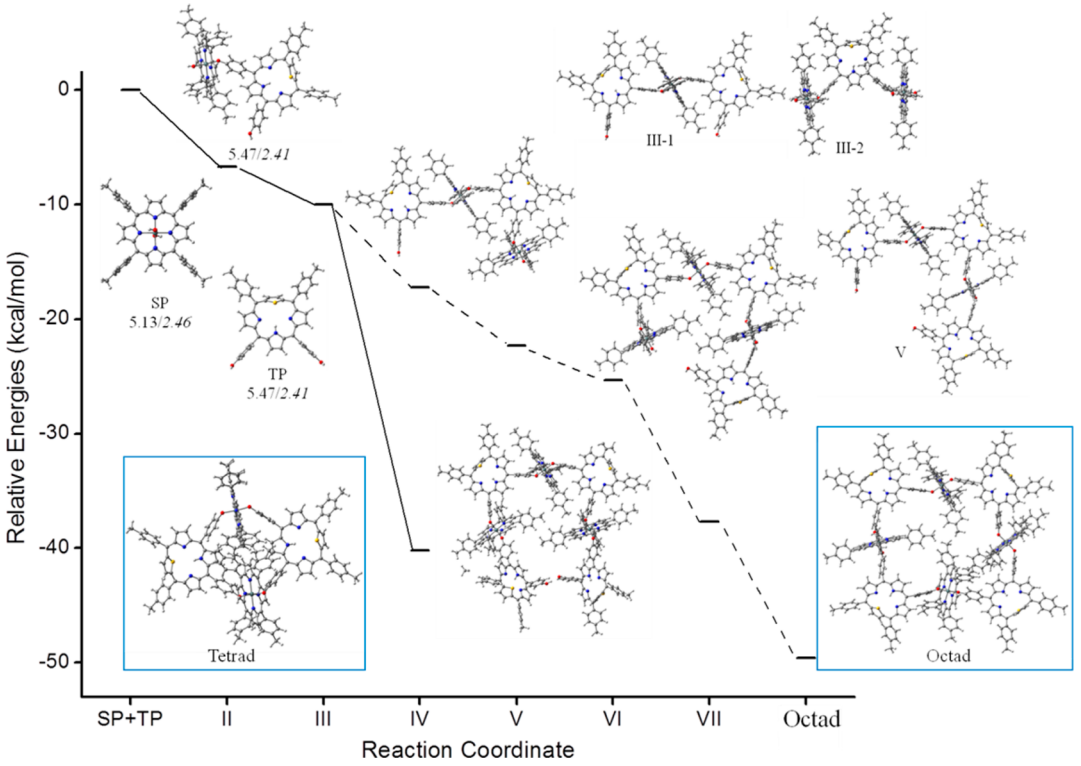

Figure 2. Schematic depicting relative energy profiles for the unit-wise addition of the formation of a tetrad and an octad calculated at M06/LanL2DZ on PM3-optimized geometries. Also shown are the energy values (in eV) for the HOMO (normal) and LUMO (italics) of **SP**, **TP**, and **II**.

that of the octad. Optimization of the geometry of the reactants and products was initially performed at the PM3 level followed by single-point-energy evaluations at M06/LanL2DZ on the PM3-optimized geometry (note that detailed DFT optimization of the cyclic tetrad using an appropriate basis set is described later). The thermodynamics calculations were performed with the *Gaussian 09* program package,[50] and unless otherwise specified, the energetics used for the discussion were obtained at the M06/LanL2DZ level. The reaction energy profiles generated for the unit-wise addition along with the optimized structures are depicted in Figure 2. The initial formation of the dyad (**II**), which involves the reaction between **SP** and **TP**, was exothermic by 6.4 kcal mol^{-1}. The next step of the formation of the triad (**III**) could proceed by attack of either **TP** on **II**, giving rise to **III-1** (reaction energy of −3.3 kcal mol^{-1}), or **SP** on **II**, giving rise to **III-2** (reaction energy of −3.6 kcal mol^{-1}). The difference of 0.3 kcal mol between the two possible pathways suggested the feasibility of the formation of both triads. To obtain further insight into the reaction, we evaluated the HOMO−LUMO energy gap between **II** and the monomers (**SP** and **TP**), respectively. The orbital energies for **SP**, **TP**, **II**, and **III-1** are depicted in Figure 2. The energy gaps, $\Delta E_{\mathrm{HOMO(II)-LUMO(TP)}}$ and $\Delta E_{\mathrm{LUMO(II)-HOMO(TP)}}$, for the formation of **III-1** were 2.45 and 2.54 eV, respectively, and the gaps, $\Delta E_{\mathrm{HOMO(II)-LUMO(SP)}}$ and $\Delta E_{\mathrm{LUMO(II)-HOMO(SP)}}$, for the formation of **III-2** were 2.50 and 2.88 eV, respectively. The lower HOMO−LUMO gap in the former suggests that **TP** attacks **II**, thereby resulting in the formation of **III-1**, which is then likely attacked by one more unit of **TP**, which could either result in the formation of a cyclic tetrad (−29.9 kcal mol^{-1}) or proceed toward the formation of an octad through the formation of an acyclic tetrad (−6.9 kcal mol^{-1}). These results suggest that the formation of a cyclic tetrad is thermodynamically preferred to that of an acyclic tetrad by about 22.2 kcal mol^{-1}. Thus, the estimated thermodynamic parameters indicate that there is a clear preference for the formation of the cyclic tetrad in comparison with the acyclic alternative, which is a necessary precursor for the formation of an octad.

1D and 2D NMR Spectroscopy of the Cyclic Tetrads. After eliminating the possibility of the formation of an octad as a product of the reaction by MALDI-TOF, DOSY, and computational studies, we proceeded to assign the ^{1}H NMR spectra of the cyclic tetrads. A comparison of the ^{1}H NMR spectrum of tetrad **1** with those of its corresponding monomers **9** and **3** is shown in Figure 3a, and the key regions of the ^{1}H−^{1}H COSY NMR spectra of tetrad **1** are shown in Figure 3b,c. The different regions of the NOESY NMR spectrum and the possible NOE correlation patterns observed for tetrad **1** are shown in Figure 4. It is clear from Figure 3a that tetrad **1** shows a large number of signals due to protons from the *β*-heterocycle and *meso*-aryl groups, which were shifted either upfield or downfield in comparison with the porphyrin monomers **9** and **3**. It should also be noted that, because of the cyclic nature of the tetrads, there could be the formation of a cavity where four *meso*-tolyl groups from the two tin(IV) porphyrin units and the two pyrrole groups from the N_3S porphyrin units in **1** or the two thiophene groups from the N_2S_2 porphyrin units in **2** were located inside the cavity. The key feature of the ^{1}H NMR spectra of the tetrads **1** and **2** was the large upfield shift for the *α*- and *β*-proton resonances of the phenoxo group of the N_3S or N_2S_2 porphyrin unit that was connected to the tin(IV) center of the metalloporphyrins. For example, the two doublets at 7.20 and 7.60 ppm that were observed for the *α*- and *β*-protons of the *meso*-hydroxyphenyl group of the N_3S porphyrin monomer **3** were shifted to the upfield region in tetrad **1** and were observed at 2.46 and 6.70 ppm, respectively. This observation

DOI: 10.1021/acs.inorgchem.7b01966
Inorg. Chem. XXXX, XXX, XXX−XXX

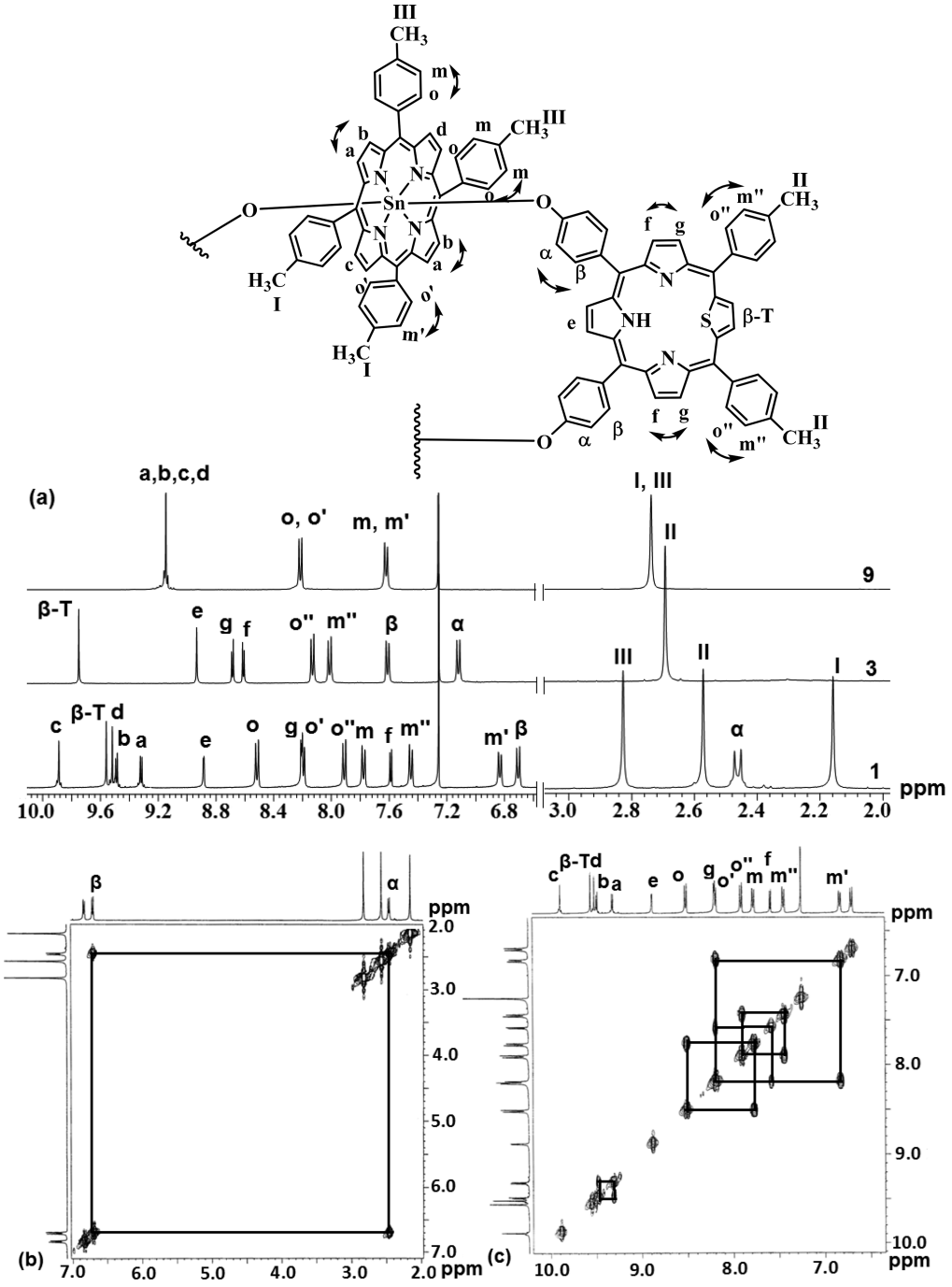

Figure 3. (a) Comparison of ^{1}H NMR spectra of tetrad **1** with its corresponding monomers **9** and **3** in $CDCl_3$. (b and c) Partial ^{1}H−^{1}H COSY NMR spectra of tetrad **1**.

was attributed to the influence of both the inherent deshielding effect of the N_3S porphyrin unit and the shielding effect of the tin(IV) porphyrin unit exhibited by the α- and β-protons (Figure 3a). The cross-peak correlation for these two sets of protons in ^{1}H−^{1}H COSY NMR confirmed this observation.

The ^{1}H NMR spectrum of tetrad **1** exhibited six doublets in the 6.82−8.51 ppm region with J couplings of 7.6−7.9 Hz corresponding to the *meso*-aryl protons of both of the porphyrin units excluding the phenoxo group of protons, four doublets at 7.58, 8.19, 9.31, and 9.48 ppm with J couplings of 4.6 Hz corresponding to the β-pyrrole protons, four singlets at 8.88, 9.51, 9.55, and 9.88 ppm corresponding to the β-pyrrole and β-thiophene protons, and three singlets at 2.16, 2.57, and 2.82 ppm corresponding to the methyl protons. The inner core NH from both of the N_3S porphyrin units displayed a singlet at −2.88 ppm corresponding to two protons. The doublet at 6.70 ppm (J = 8.2 Hz) that was attributed to the type β proton of the phenoxo connector displayed NOE correlations with a singlet and a doublet at 8.88 and 7.58 ppm (J = 4.6 Hz), respectively. The same doublet peak at 7.58 ppm showed a COSY correlation to a doublet at 8.19 ppm (J = 4.6 Hz). These correlations revealed that the singlet at 8.88 ppm was due to type e proton resonance from the β-pyrrole protons of the N_3S porphyrins flanked by two phenoxo linkers. The doublets at 7.58 and 8.19 ppm were attributed to type f and g proton resonances, respectively, from the β-pyrrole protons of the N_3S

DOI: 10.1021/acs.inorgchem.7b01966
Inorg. Chem. XXXX, XXX, XXX−XXX

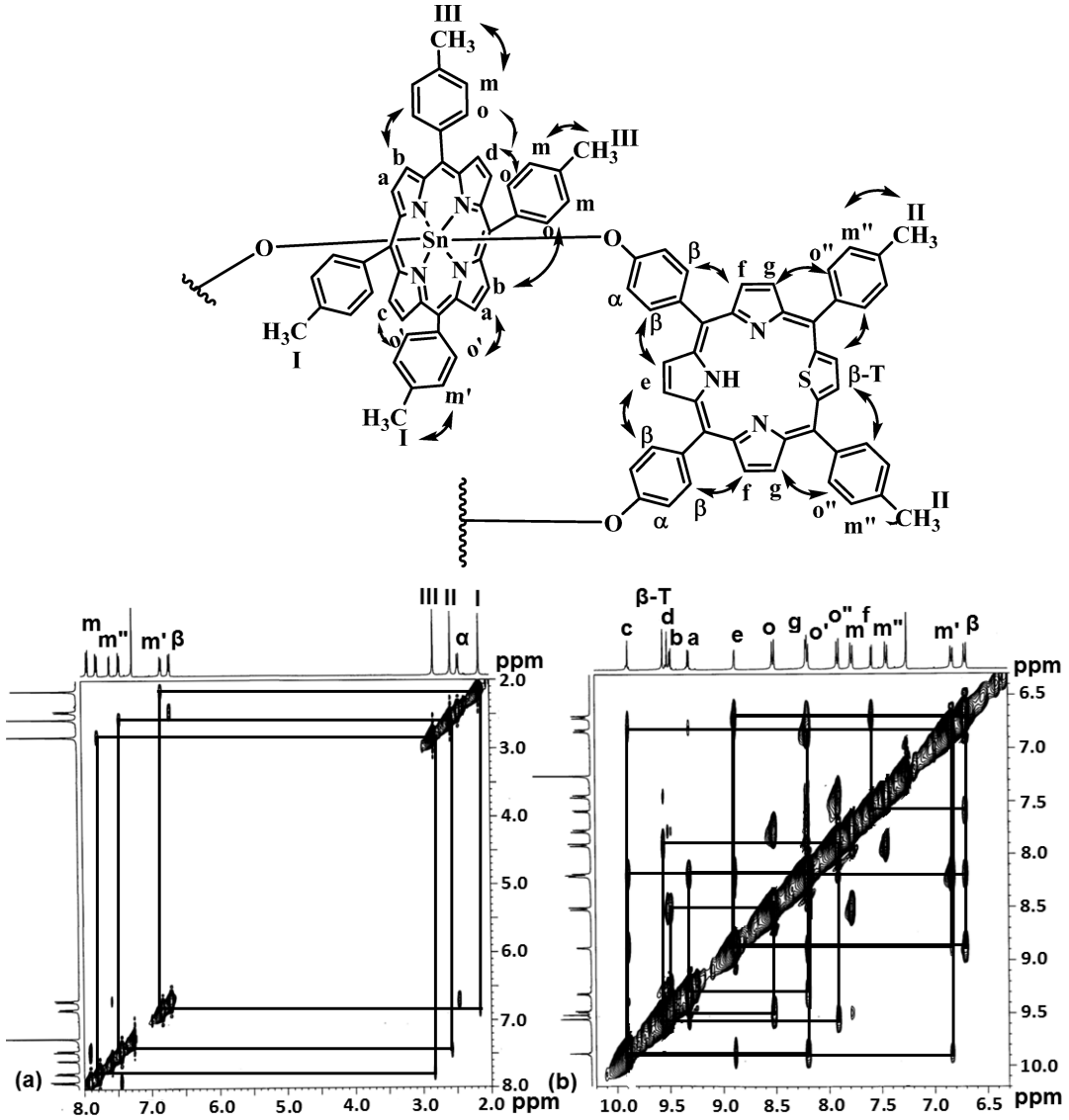

Figure 4. Partial $^{1}H-^{1}H$ NOESY NMR spectra of tetrad **1**.

porphyrin units that were located between the phenoxo linker and tolyl groups. The singlet peak at 9.55 ppm that corresponded to four protons was assigned to the *β*-thiophene proton resonance of the N_3S porphyrin units. This singlet at 9.55 ppm showed a NOE correlation with a doublet at 7.90 ppm (J = 7.9 Hz), which, in turn, showed a COSY correlation with a doublet at 7.44 ppm (J = 7.9 Hz). A NOE correlation was also observed between the doublet at 7.44 ppm (J = 7.9 Hz) and the singlet at 2.57 ppm. Hence, following these observations, we assigned the doublets at 7.90 and 7.44 ppm to type o″ and m″ proton resonances, respectively, and the singlet peak at 2.57 ppm to the methyl protons of type II from the *meso*-tolyl groups of the N_3S porphyrin units.

The singlet peak at 2.16 ppm displayed a NOE correlation to a doublet at 6.83 ppm (J = 7.6 Hz), which, in turn, showed a COSY correlation to a doublet at 8.20 ppm (J = 7.6 Hz). The same doublet at 8.20 ppm also showed two NOE correlations: one with a doublet at 9.31 ppm (J = 4.6 Hz) and the second with a singlet at 9.88 ppm. Also, the doublet at 9.31 ppm showed a COSY correlation with a doublet at 9.48 ppm. These observations indicate that the doublets at 6.83 and 8.20 ppm were due to type m′ and o′ proton resonances, respectively, from the *meso*-tolyl groups of the tin(IV) porphyrin units present inside the cavity of the cyclic tetrad. The doublets at 9.31 and 9.48 ppm and the singlet at 9.88 ppm were attributed to the *β*-proton resonances of types a−c, respectively. The singlet at 2.16 ppm was assigned to CH_3 protons of type I from the *meso*-tolyl groups of the tin(IV) porphyrins that were located inside the cavity of the cyclic tetrad.

The doublet peak at 8.51 ppm (J = 7.9 Hz) showed a NOE correlation with a singlet at 9.51 ppm and a COSY correlation with a doublet at 7.77 ppm (J = 7.9 Hz). The doublet at 7.77 ppm also showed a NOE correlation with a singlet at 2.82 ppm. These observations indicated that the doublets at 8.51 and 7.77 ppm were due to type o and m protons, respectively, from the tolyl groups of the tin(IV) porphyrin units that were present outside the cavity of the cyclic tetrad. The singlet at 9.51 ppm was due to type d *β*-pyrrole protons. The singlet peak at 2.82 ppm was unambiguously assigned to type III methyl protons from the *meso*-tolyl groups of the tin(IV) porphyrin units that were located on the outer periphery of the cyclic tetrad. The tetrad **2** also displayed similar ^{1}H NMR resonances that were assigned by adopting a approach based on 1D and 2D NMR spectra similar to that described for tetrad **1** (Figures S9−S11).

DOI: 10.1021/acs.inorgchem.7b01966
Inorg. Chem. XXXX, XXX, XXX−XXX

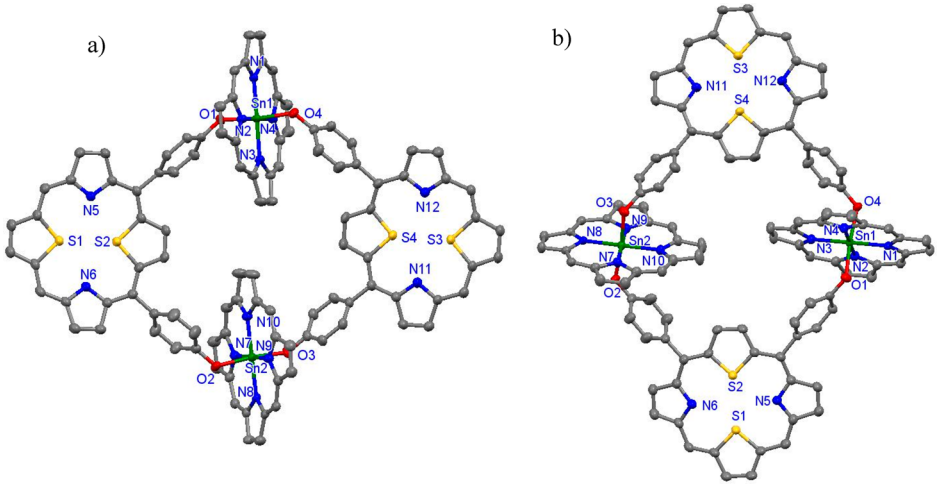

Figure 5. Single-crystal X-ray structure of tetrad **2**: (a) top view; (b) side view. Thermal ellipsoids are drawn at 50% probability. The hydrogen atoms and *meso* aryl groups were removed for clarity.

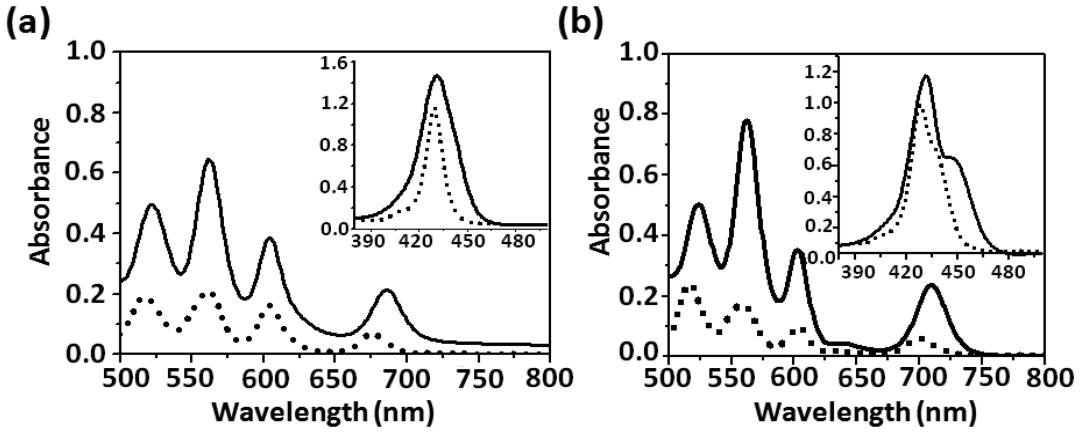

Figure 6. Q and Soret band (inset) absorption spectra of tetrads (a) **1** and (b) **2** (solid line) with a 1:1 mixture of monomers (dotted line) recorded in toluene.

Table 1. Absorption Parameters for Tetrads 1 and 2 and the Corresponding Monomers

	λ, nm (log ε, M^{-1} cm^{-1})					
compd	Soret band		Q bands			
9	427		562 (4.51)	603 (4.46)		
3	430 (6.06)	515 (4.51)	551 (4.15)		618 (3.74)	675 (4.14)
1	431 (6.27)	521 (4.69)	562 (4.81)	604 (4.58)		685 (4.32)
1:1 mixture of **3** and **9**	427 (6.07)	516 (4.28)	562 (4.32)	604 (4.20)		675 (3.85)
4	437 (6.00)	515 (4.50)	551 (4.13)		634 (3.37)	699 (3.89)
2	431 (6.20), 448 (5.80)	523 (4.70)	562 (4.89)	602 (4.54)		710 (4.38)
1:1 mixture of **4** and **9**	427 (6.07), 439 (5.72)	516 (4.23)	561 (4.35)	603 (4.21)		700 (3.57)

Single-Crystal X-ray Crystallography. The crystals of compound **2** suitable for single-crystal X-ray diffraction were obtained by the slow diffusion of hexanes into a CH_2Cl_2 solution of **2** over a period of 2 weeks. The crystallographic data are presented in Table S1. Compound **2** crystallized in the triclinic space group $P\bar{1}$ along with a solvated molecule of dichloromethane. The prospective view of the crystal structure is shown in Figure 5. The crystal structure explicitly corroborates the formation of a tetrad in which two *cis*-dihydroxyphenyl N_2S_2 porphyrins are axially ligated to two tin(IV) porphyrins, as predicted by DOSY NMR and computational studies. The tin(IV) porphyrins present a perfect octahedral geometry with a planar porphyrin core, whereas the N_2S_2 porphyrin core is slightly ruffled (5°) because of relatively large sulfur atoms. In the tetrad, the two tin(IV) porphyrins are geometrically placed at an angle of 49° with each other in order to minimize the steric repulsions that arise from the corresponding *meso*-aryl groups (Figure S12). The two axially coordinated N_2S_2 porphyrins are positioned orthogonally at angles of 79° and 52° with respect to the mean planes of tin(IV) porphyrins. The average "Sn−N" and "Sn−O" bond distances are 2.09 and 2.03 Å, while the "Sn−O−C" bond angles are 124° and 127°, which are in line with those of the reported[51] tin(IV) porphyrin based systems. Thus, comprehensive analysis of the bond angles and distances reveals that the positions of two hydroxyl groups of the (12.5 Å) N_2S_2

DOI: 10.1021/acs.inorgchem.7b01966
Inorg. Chem. XXXX, XXX, XXX−XXX

porphyrin, which are well separated by a distance of 12.2 Å, are crucial in order to construct a less constrained and stable cyclic tetrad rather than an octad. In the crystal packing of **2**, the two N_2S_2 porphyrins of the tetrad overlap with the N_2S_2 porphyrins of the adjacent tetrad, leading to an extended one-dimensional stack. However, the $\pi-\pi$ distance was measured to be slightly longer (4.0 Å) than the usual acceptable $\pi-\pi$ bond distances (3.3−3.8 Å; Figure S12). On the other hand, no such stacking interactions were noticed between the tin(IV) porphyrin units of the tetrad, which indicates that the tetrads are stabilized by secondary interactions such as C−H···π and C−H···O and other weak (*meso*-aryl−*meso*-aryl) $\pi-\pi$ interactions in the solid state.

Electrochemical and Photophysical Investigations of the Cyclic Tetrads. A comparison of the Q and Soret band regions of the absorption spectra of the cyclic tetrads **1** and **2** and the corresponding 1:1 mixture of monomers in toluene are shown in parts a and b of Figure 6, respectively. The corresponding spectral parameters are presented in Table 1. The absorption spectra of tetrads **1** and **2** displayed features of both of the constituent monomers and appeared as a near-superimposition of their absorption spectra with minimal shifts in the peak positions. For example, the absorption spectrum of tetrad **2** showed bands at 431, 448, 523, 562, 602, and 710 nm. Among these, the bands at 431, 562, and 602 nm were due to a contribution from the tin(IV) porphyrin unit and the bands at 448, 523, and 710 nm arise from the 21,23-dithiaporphyrin unit. The absorption bands of tetrads **1** and **2** were slightly red-shifted with enhanced molar extinction coefficient values in comparison with a 1:1 mixture of the constituted monomers.

The cyclic voltammograms of the cyclic tetrads **1** and **2** and the corresponding monomers in dichloromethane with tetrabutylammonium perchlorate (TBAP) as the supporting electrolyte are presented in Table 2. The reduction waves of tetrads **1** and **2** are shown in parts a and b of Figure 7, respectively. The redox potentials of tetrads **1** and **2** were in the same range as those of the corresponding monomers. For example, tetrad **1** displayed three oxidation peaks at 0.95, 1.28, and 1.42 V and three reduction peaks at −0.92, −1.11, and −1.34 V. The oxidation peaks at 0.95 and 1.28 V were attributed to the 21-thiaporphyrin unit, and the oxidation peak at 1.42 V was due to the tin(IV) porphyrin unit. The reduction potentials that were observed for tetrad **1** were also attributed to contributions from both of the constituent monomers because they possess similar reduction potentials. Thus, the electrochemical studies indicate that the redox properties of the cyclic tetrads **1** and **2** did not vary significantly in comparison with the corresponding monomers.

Table 2. Redox Potentials (V) for Tetrads 1 and 2 and the Corresponding Monomers

	$E_{1/2}$, V vs SCE					
compd	oxidation			reduction		
9	1.41			−0.97		−1.36
3		1.27	0.94	−1.04	−1.23	
1	1.42	1.28	0.95	−0.92	−1.11	−1.34
4		1.26	0.94	−0.97		−1.36
2	1.36	1.23	0.96	−1.00		−1.38

The steady-state fluorescence properties of tetrads **1** and **2** in toluene are presented in Table 3. Tetrads **1** and **2** were excited at 515 and 560 nm, respectively, where thiaporphyrin and tin(IV) porphyrin display relatively strong absorption peaks. A comparison of the fluorescence spectra of tetrad **1** and a 1:1 mixture of the corresponding monomers at an excitation wavelength of 560 nm, where the tin(IV) porphyrin unit is a dominant absorber, is shown in Figure 8. When tetrads **1** and **2** were excited at 515 nm, where the thiaporphyrin unit is a dominant absorber, the fluorescence that was observed is exclusively from the thiaporphyrin unit. However, with

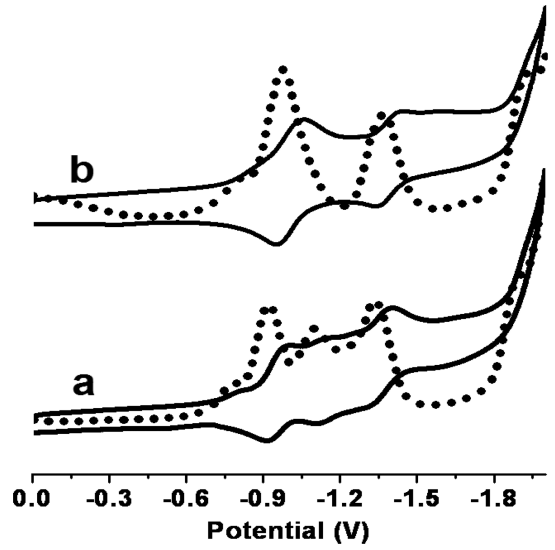

Figure 7. Overlay of the reduction waves of the cyclic voltammograms (thick line) and differential pulse voltammograms (dotted line) of tetrads (a) **1** and (b) **2** recorded in dichloromethane containing 0.1 M TBAP as the supporting electrolyte (scan rate 50 mV s^{-1}).

Table 3. Photophysical Data for Tetrads 1 and 2 and the Corresponding Monomers

compd	λ_{ex}, nm	Φ_{N2XYP}	% Q	Φ_{SnP}	% Q	Φ_{ENT},[a] %
$SnTTP(OH)_2$ (**9**)	560			0.025		
N_3STTP	515	0.017				
1	560	0.00033	98	0.00065	97	57
	515	0.0012	92			
N_2S_2TTP	515	0.007				
2	560	0.00069	97	0.00035	99	62
	515	0.0029	60			

[a] Φ_{ENT} % = $[1 - F_{DA}/F_D] \times 100\%$

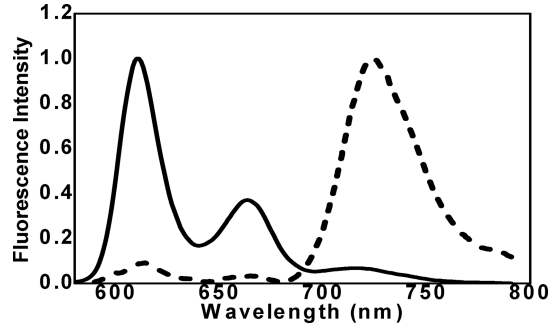

Figure 8. Comparison of the normalized emission spectra of tetrad **1** (dashed line) and a 1:1 mixture of monomers **9** and **3** (solid line) recorded in toluene at an excitation wavelength, λ_{ex}, of 560 nm.

DOI: 10.1021/acs.inorgchem.7b01966
Inorg. Chem. XXXX, XXX, XXX−XXX

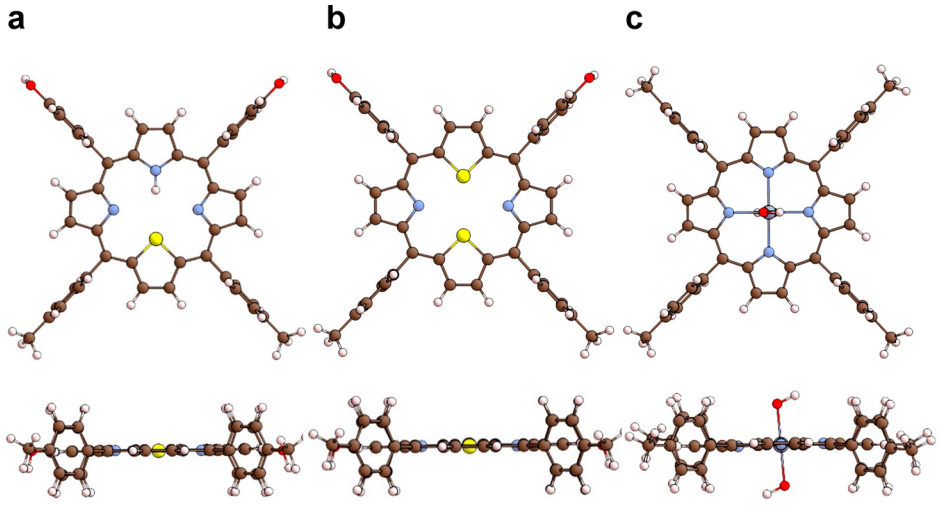

Figure 9. Relaxed equilibrium DFT structure of the monomers (a) **3**, (b) **4**, and (c) **9**. Also shown is a side view of each monomer. The carbon, hydrogen, nitrogen, oxygen, sulfur, and tin atoms are shown in brown, pink, blue, red, yellow, and gray, respectively.

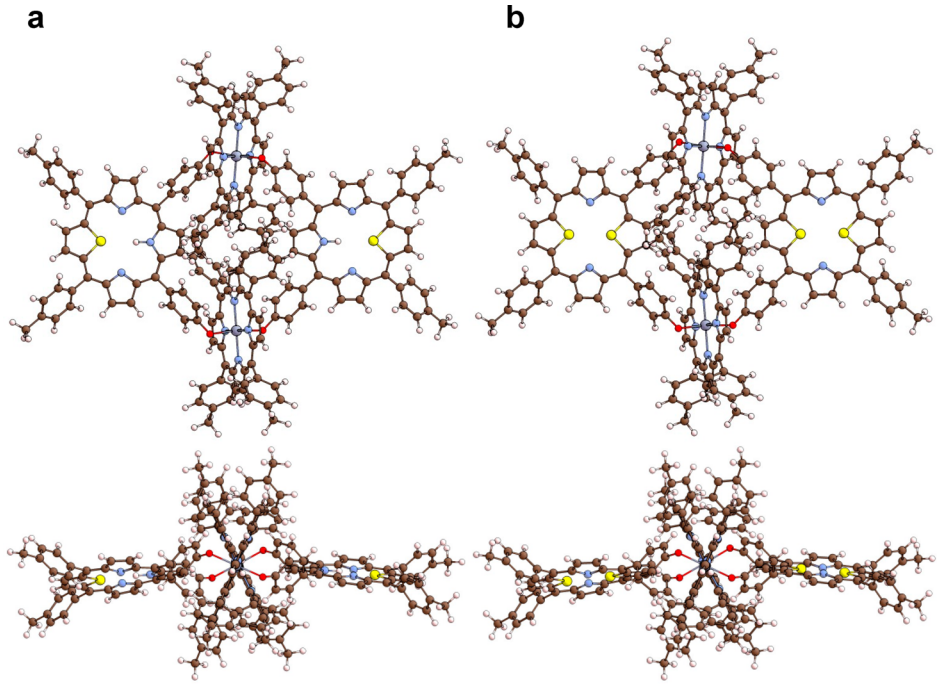

Figure 10. Relaxed equilibrium DFT structure of the tetrads (a) **1** and (b) **2**. Also shown is a side view of each tetrad. The carbon, hydrogen, nitrogen, oxygen, sulfur, and tin atoms are shown in brown, pink, blue, red, yellow, and gray, respectively.

excitation at 515 nm, the quantum yield of the thiaporphyrin unit in tetrads **1** and **2** was substantially decreased in comparison with the monomeric thiaporphyrin because of coordination to two heavy tin(IV) atoms. Interestingly, when tetrads **1** and **2** were excited at 560 nm, where the tin(IV) porphyrin unit is a dominant absorber, the emission from the tin(IV) porphyrin unit was quenched significantly and a major emission was observed from the thiaporphyrin unit. This was very clear in tetrad **2**, where the emission from the 21,23-dithiaporphyrin unit was dominant and the emission from the tin(IV) porphyrin unit was quenched significantly (Figure S13). The excitation spectra of tetrads **1** and **2** that were recorded at 710 and 720 nm, respectively, closely resembled the corresponding absorption spectra of tetrads **1** and **2**. Furthermore, the 1:1 mixture of the corresponding monomers of tetrads **1** and **2** upon excitation at 560 nm showed dominant emission from the tin(IV) porphyrin monomer, with a negligible emission from the thiaporphyrin monomer. All of these observations suggest that, in the cyclic tetrads **1** and **2**, upon excitation at 560 nm, there is a possibility of singlet energy transfer from the tin(IV) porphyrin unit to the thiaporphyrin unit. Although the decrease in the fluorescence intensity of the tin(IV) porphyrin unit in tetrads **1** and **2** upon excitation at 560 nm was largely attributed to energy transfer from the tin(IV) porphyrin unit to the thiaporphyrin unit, we cannot rule out the contribution of photoinduced electron transfer between the tin(IV) porphyrin and thiaporphyrin units in tetrads for the same. However, detailed ultrafast photophysical studies are required to quantify the energy-transfer dynamics in the cyclic tetrads **1** and **2**.

DOI: 10.1021/acs.inorgchem.7b01966
Inorg. Chem. XXXX, XXX, XXX−XXX

Table 4. Planarity of the Porphyrin Macrocycle and the Dihedral Angles of *meso*-Aryl Substituents in Tetrads 1 and 2 and the Corresponding Monomers

	species						
				tetrad 1		tetrad 2	
parameter	3	4	9	N_3S	Sn	N_2S_2	Sn
Δ 24	0.00	0.00	0.00	0.078	0.035	0.088	0.035
Δ N	−0.004	−0.002	0.005	0.074	0.024	0.099	0.029
Sn			0.01		0.019		0.021
hetero ring	0.6	0.6	1.3	5.2	2.3	6.0	2.3
meso-aryl	85.1	84.7	88.0	59.4	76.0	56.2	76.0
planar dihedral				25.7	49.6	24.4	51.5

Quantum-Mechanical DFT and TD-DFT Calculations. The monomers (**3**, **4** and **9**) and tetrads (**1** and **2**) were investigated by quantum-mechanical DFT calculations. The relaxed equilibrium DFT structures are presented in Figures 9 and 10, and the corresponding structural parameters are shown in Tables 4 and 5. The bond lengths and angles in the relaxed DFT structures of the monomers (Figure 9 and Tables 4 and 5) are in good agreement with the respective X-ray crystal structures[52−58] and calculated structures in the literature.[59−63] A notable feature of the tin(IV) ion in monomer **9** is that it displayed a distorted octahedral geometry, where the O−Sn−O bond was tilted toward the mean plane of the macrocycle (Table 5), which is also in agreement with X-ray crystal and computational structures.[57,58,62]

Table 5. Interatomic Distances in Tetrads 1 and 2 and the Corresponding Monomers

	species				
parameter	9	3	4	tetrad 1	tetrad 2
Sn−Sn				12.7	12.8
O−O		12.9	13.0	13.05	13.15
Sn−O	2.04			2.07	2.07
Sn−N	2.13			2.12	2.12
O−Sn−O	180			174	174
O−Sn−O tilt	3			3	3

In the relaxed DFT structures of tetrads **1** and **2**, the two thiaporphyrin units that were coordinated to the tin(IV) porphyrin created the appearance of a cavity where all four porphyrin molecules of the tetrad are in van der Waals contact with each other (Figure 10). The interporphyrin distances were ≤5 Å, which are in agreement with the crystallographic data of **2**. Moreover, the relaxed tetrad structures resembled a ruffled ring where the angles between the mean plane of thiaporphyrin and the respective tin(IV) porphyrin were ∼25° and ∼50°, respectively (Table 4). The planarity of each porphyrin subunit decreased upon formation of the tetrad, which is in agreement with the observed ^{1}H NMR chemical shifts. The formation of both tetrads resulted in changes in the dihedral angles, planarity, and coordination geometry of the tin(IV) ion that are listed in Tables 4 and 5.

Shown in Figures S14−S16 are the charge-density distributions of the frontier molecular orbitals of monomers **3**−**5**, respectively, which were calculated from the corresponding relaxed DFT structures. It was observed that each monomer exhibited standard Gouterman-type orbitals. The LUMOs of monomers **3** and **4** displayed charge density on the sulfur atoms, which was absent in the LUMO+1 orbital (Figures S14 and S15). This is in agreement with the bathochromic shift that was observed for the low-energy Q bands (and absent in the higher-energy bands). Similarly, the corresponding HOMO−LUMO gap for the thiaporphyrin and tin(IV) porphyrin units of tetrad **1** was in agreement with the bathochromic shifts observed in the absorption spectrum.

The calculated charge-density distributions of tetrads **1** and **2** are shown in Figures S17 and S18, respectively. As can be seen in Figures S17 and S18, the charge density was primarily localized on the monomeric units. Moreover, the frontier molecular orbitals of tetrads **1** and **2** were relatively similar to minor differences. Both of the tetrads exhibited a similar charge-density distribution in the unoccupied orbitals, where the LUMO and LUMO+1 orbitals resembled the tin(IV)-porphyrin and the LUMO+2 and LUMO+3 resembled the thiaporphyrin. The ordering of the LUMO of the thiaporphyrin subunits is preserved between the monomers and tetrads. In contrast, the order of the occupied orbitals was switched in the tetrads where the HOMOs of tetrads **1** and **2** resembled the HOMO of the thiaporphyrin.

The relaxed DFT structures of the monomers and tetrads were also studied by TD-DFT to understand the bathochromic shifts that were observed in the experimental absorption spectra. As can be seen in Figures S19 and S20, the Q bands of the absorption spectra predicted by TD-DFT are in qualitative agreement with the experimental spectra shown in Figure 6. The calculated spectra predicted that the Q bands of the thiaporphyrin unit were shifted by ∼15−25 nm, whereas there was no observable shift of the tin(IV)porphyrin bands upon tetrad formation, which is in agreement with the experimental spectra.

CONCLUSIONS

In conclusion, syntheses of the first examples of tin(IV) porphyrin based cyclic arrays **1** and **2** containing tin(IV) porphyrin and thiaporphyrin units were reported. These arrays were constructed exclusively by utilizing the oxophilic nature of tin(IV) porphyrins. These arrays were confirmed as cyclic tetrads based on MALDI-TOF MS, DOSY NMR, computational, and X-ray crystallographic studies. These cyclic tetrads were stable in solution as well as under redox conditions. The preliminary photophysical studies indicated a possible energy transfer within the cyclic systems, and detailed studies are currently underway in our laboratory. The DFT and TD-DFT studies on the monomers and tetrads indicated that the porphyrin subunits exhibit small minimum mixing of orbitals. Moreover, formation of the tetrad produces small perturbations of the porphyrin macrocyclic structure, yielding spectra similar to those of the monomers.

DOI: 10.1021/acs.inorgchem.7b01966
Inorg. Chem. XXXX, XXX, XXX−XXX

EXPERIMENTAL SECTION

Chemicals. All general chemicals and solvents were procured from SD Fine Chemicals, India. Column chromatography was performed using silica gel and basic alumina obtained from Sisco Research Laboratories, India. All of the solvents used were of analytical grade and were purified and dried by routine procedures immediately before use.

Instrumentation. ^{1}H NMR spectra were recorded with a Bruker 400 MHz instrument using tetramethylsilane as an internal standard. ^{1}H−^{1}H COSY, NOESY, and DOSY NMR experiments were performed on a Bruker 400 MHz instrument. All NMR measurements were carried out at room temperature in deuterated chloroform ($CDCl_3$). Absorption and steady-state fluorescence spectra were recorded on PerkinElmer Lambda-35 and Varian Cary-Eclipse instruments, respectively. The concentrations used for the absorption study were 1×10^{-6} and 1×10^{-5} M for the Soret and Q bands, respectively. The concentration used for the steady-state fluorescence study was 1×10^{-6} M. The fluorescence quantum yields (Φ_f) were estimated from the emission and absorption spectra by a comparative method. The time-resolved fluorescence decay measurements were carried out at magic angle using a picosecond diode-laser-based time-correlated single-photon-counting (TCSPC) fluorescence spectrometer from IBH, Swindon, U.K. MALDI-TOF MS spectra were recorded from a MALDI-TOF Spec-2E instrument manufactured by Micromass, Wilmslow, U.K. Cyclic and differential-pulse voltammetric studies were carried out on a BAS electrochemical system utilizing the three-electrode configuration consisting of glassy carbon (working), platinum wire (auxiliary), and saturated calomel (reference) electrodes in dry dichloromethane using 0.1 M TBAP as the supporting electrolyte.

Single crystals of suitable size for the X-ray diffractometer were selected under a microscope and mounted on the tip of a glass fiber, which was positioned on a copper pin. The X-ray data for tetrad **2** (CCDC 1564602) were collected on a Bruker Kappa CCD diffractometer, employing graphite-monochromated Mo Kα radiation at 200 K and the θ−2θ scan mode. The space group for tetrad **2** was determined on the basis of systematic absences and intensity statistics, and the structure of tetrad **2** was solved by direct methods using *SIR92* or *SIR97* and refined with *SHELXL-97*.[64]

Dihydroxy[5,10,15,20-tetrakis(*p*-tolyl)porphyrinato]tin(IV) [9; Sn^{IV}TTP(OH)$_2$]. Compound **9** was synthesized by treating H_2TTP (3 mmol) in $CHCl_3$ with 10 equiv of $SnCl_2 \cdot 2H_2O$. The progress of the reaction was monitored by TLC and absorption spectroscopy. After the formation of a new spot on the TLC spectrum and the disappearance of the starting materials, the reaction was stopped and subjected to basic alumina column chromatography. The required compound **9** was collected in 90% yield as a purple solid.[49] Mp: >300 °C. ^{1}H NMR (400 MHz, $CDCl_3$): δ −7.43 (s, 2H, br, axial OH), 2.70 (s, 12H, CH_3), 7.61 (d, J = 7.8 Hz, 8H, Ar), 8.20 (d, J = 7.8 Hz, 8H, Ar), 9.13 (s, satellite, J = 10.7 Hz, 8H, β-pyrrole).

5,10-Bis(*p*-hydroxyphenyl)-15,20-bis(*p*-tolyl)-21-dithiaporphyrin (3). The required porphyrin **3** was synthesized by condensing 2,5-bis(*p*-tolylhydroxyl)methylthiophene (**5**; 12.29 mmol, 1.25 mL) and *p*-hydroxybenzaldehyde (4.09 mmol, 500 mg) with pyrrole (16.39 mmol, 1.11 mL) in propionic acid at 70 °C for about 4 h. The crude compound was showing about six spots on the TLC spectrum, which was purified by silica gel column chromatography using a CH_2Cl_2/petroleum ether mixture (2:3) as the eluent to afford **3** in 10% yield. Mp: >300 °C. ^{1}H NMR (400 MHz, $CDCl_3$): δ −2.69 (s, 1H, NH), 2.70 (s, 6H, CH_3), 7.18 (d, J = 7.9 Hz, 4H, Ar), 7.61 (d, J = 7.9 Hz, 4H, Ar), 8.10 (d, J = 8.2 Hz, 4H, Ar), 8.18 (d, J = 8.2 Hz, 4H, Ar), 8.60 (d, J = 4.60 Hz, β-pyrrole), 8.70 (d, J = 4.60 Hz, β-pyrrole), 8.90 (s, 2H, β-pyrrole), 9.75 (s, 2H, β-thiophene). ES-MS. Calcd for $C_{46}H_{33}N_3O_2S$ ([M]$^+$): m/z 691.8. Obsd: m/z 691.5.

5,10-Bis(*p*-methoxyphenyl)-15,20-bis(*p*-tolyl)-21,23-dithiaporphyrin (6). The samples of 2,5-bis(*p*-anisyl)-hydroxymethylthiophene (**8**; 0.5 g, 1.53 mmol) and 16-thiatripyrrane (0.65 g, 1.53 mmol) were dissolved in dichloromethane (300 mL), and the reaction flask was degassed with nitrogen for 10 min with stirring. The condensation was initiated by adding $BF_3 \cdot OEt_2$ (0.4 mL of a 2.5 M solution) while the reaction mixture was stirred at room temperature for 1 h under a nitrogen atmosphere. 2,3-Dichloro-5,6-dicyanobenzoquinone (DDQ; 0.33 g, 1.53 mmol) was then added, and the reaction mixture was stirred in air for an additional 1 h. The solvent was removed under reduced pressure, and the crude compound was purified by silica gel column chromatography using petroleum ether/dichloromethane (60:40) to afford porphyrin **6**. Yield: 20%. Mp: >300 °C. ^{1}H NMR (400 MHz, $CDCl_3$): δ 2.70 (s, 6H, CH_3), 4.10 (s, 6H, OCH_3), 7.32 (d, J = 8.7 Hz, 4H, Ar), 7.61 (d, J = 7.8 Hz, 4H, Ar), 8.09 (d, J = 8.2 Hz, 4H, Ar), 8.12 (d, J = 7.8 Hz, 4H, Ar), 8.68 (s, 4H, β-pyrrole), 9.68 (s, 4H, β-thiophene). HRMS (ES$^+$). Calcd for $C_{48}H_{36}N_2O_2S_2$: m/z 736.9416 ([M]$^+$). Found: m/z 737.2287 ([M + H]$^+$).

5,10-Bis(*p*-hydroxyphenyl)-15,20-bis(*p*-tolyl)-21,23-dithiaporphyrin (4). Compound **4** was synthesized by refluxing porphyrin **6** (0.1 g, 14 mmol) in 30 mL of hydrogen bromide/water (49%) for 4 h. The reaction mixture was extracted with dichloromethane and washed several times with water and a dilute ammonia solution (25%, v/v). The organic layer was evaporated under reduced pressure and subjected to silica gel column chromatographic purification using dichloromethane to afford pure **9**. Yield: 68%. Mp: >300 °C. ^{1}H NMR (400 MHz, $CDCl_3$): δ 2.70 (s, 6H, CH_3), 7.20 (d, J = 9.0 Hz, 4H, Ar), 7.61 (d, J = 7.8 Hz, 4H, Ar), 8.10 (d, J = 8.2 Hz, 4H, Ar), 8.19 (d, J = 7.8 Hz, 4H, Ar), 8.70 (s, 4H, β-pyrrole), 9.71 (s, 4H, β-thiophene). HRMS (ES$^+$). calcd for $C_{46}H_{32}N_2O_2S_2$ ([M]$^+$): m/z 708.8885. Found: m/z 709.2002 ([M + H]$^+$).

General Synthesis of Tetrads 1 and 2. Tetrads **1** and **2** were synthesized by refluxing 1 equiv of **9** with 1 equiv of **3** and **4**, respectively, in dry benzene for 12 h under a nitrogen atmosphere. The solvent was evaporated under reduced pressure, and the resulting residue was subjected to an alumina column. The desired product was eluted with petroleum ether/dicholoromethane (30:70) to afford tetrads **1** and **2** in 65−70% yield.

Tetrad 1. Yield: 65%. ^{1}H NMR (400 MHz, $CDCl_3$): δ −2.88 (s, 2H, inner NH), 2.16 (s, 12H, CH_3 type I), 2.46 (d, J = 8.24 Hz, 8H, phenoxo type α), 2.57 (s, 12H, CH_3 type II), 2.82 (s, 12H, CH_3 type III), 6.70 (d, J = 8.24 Hz, 8H, phenoxo type β), 6.83 (d, J = 7.64 Hz, 8H, Ar, type m′), 7.44 (d, J = 7.88 Hz, 8H, Ar, type m″), 7.58 (d, J = 4.68 Hz, 4H, β-pyrrole N_3S unit, type f), 7.77 (d, J = 7.92 Hz, 8H, Ar, type m), 7.90 (d, J = 7.88 Hz, 8H, Ar, type o″), 8.19 (d, J = 4.60 Hz, 4H, β-pyrrole N_3S unit, type g), 8.20 (d, J = 7.76 Hz, 8H, Ar, type o′), 8.51 (d, J = 7.88 Hz, 8H, Ar, type o), 8.88 (s, 4H, β-pyrrole N_3S unit, type e), 9.31 (d, J = 4.60 Hz, 4H, β-pyrrole SnP, type a), 9.48 (d, J = 4.60 Hz, 4H, β-pyrrole SnP, type b), 9.51 (s, 4H, β-pyrrole SnP, type d), 9.55 (s, 4H, β-thiophene N_3S), 9.88 (s, 4H, β-pyrrole SnP, type c). MALDI-TOF MS. Calcd: m/z 2954.7 ([M]$^+$). Found: m/z 2956.7 (M$^+$ + 2).

Tetrad 2. Yield: 70%. ^{1}H NMR (400 MHz, $CDCl_3$): δ 2.06 (s, 12H, CH_3 type I), 2.52 (d, J = 7.2 Hz 8H, phenoxo type α), 2.59 (s, 12H, CH_3 type II), 2.83 (s, 12H, CH_3 type III), 6.77 (d, J = 7.2 Hz, 8H, phenoxo type β), 6.78 (d, J = 7.4 Hz, 8H, Ar, type m′), 7.46 (d, J = 7.9 Hz, 8H, Ar, type m″), 7.54 (d, J = 4.7 Hz, 4H, β-pyrrole N_3S unit, type f), 7.78 (d, J = 8.0 Hz, 8H, Ar, type m), 7.92 (d, J = 7.9 Hz, 8H, Ar, type o″), 8.16 (d, J = 7.9 Hz, 8H, Ar, type o′), 8.23 (d, J = 4.6 Hz, 4H, β-pyrrole N_3S unit, type g), 8.51 (d, J = 8.0 Hz, 8H, Ar, type o), 9.27 (d, J = 4.6 Hz, 4H, β-pyrrole SnP, type a), 9.47 (d, J = 4.6 Hz, 4H, β-pyrrole SnP, type b), 9.51 (s, 4H, β-pyrrole SnP, type d), 9.53 (s, 4H, β-thiophene N_3S), 9.62 (s,4H, β-thiophene N_3S), 9.89 (s, β-pyrrole SnP, type c). MALDI-TOF MS. Calcd: ([M]$^+$): m/z 2988.8. Found: m/z 2990.6 (M$^+$ + 2).

DFT Calculations of Monomers 3, 4, and 9 and Tetrads 1 and 2. The geometry optimizations were performed using the Vienna ab initio software package (*VASP*).[65] The PBE functional[66] and the projected-augmented-wave[67] potential method embedded in the *VASP* code were used to describe the core−valence electron interactions. Long-range dispersion interactions were described using the DFT-D2 method of Stefan Grimme.[68] The initial positions for monomers **3**, **4**, and **9** were constructed and relaxed in the *Avogadro* software package.[69] Tetrads **1** and **2** were constructed from their respective monomers and subjected to simulated annealing. Subsequently, the

DOI: 10.1021/acs.inorgchem.7b01966
Inorg. Chem. XXXX, XXX, XXX−XXX

structures were relaxed in *Avogadro*.[69] The resulting coordinates were transposed to the center of a periodic box, and a vacuum space of ~0.5 nm was provided to prevent electronic interactions between periodic cells. The spin-polarized molecular wave functions of the relaxed structures were decomposed into energy bands of valence electrons and compared to the results obtained in the succeeding sentences. The electronic structure calculations were performed on relaxed structures using DFT at the B3LYP/6-31G(d)[70] level of theory and the RIJCOSX[71−74] and Newton−Rhapson self-consistent-field approximations using the ORCA electron structure package.[75−77] The LANL2DZ effective core potential basis set[78−80] was used to for S and Sn, and the def2/J[81] auxiliary basis set was applied to all elements. Solvent effects were approximated by the conductor-like polarization continuum model[82] solvation model using the refractive index and dielectric of toluene. TD-DFT[83−86] was used to predict the electronic transitions and absorption spectra of monomers **3**, **4**, and **9** and tetrads **1** and **2**. The simulated spectra were generated using the wavelengths of absorption predicted in the TD-DFT calculations by superimposing Gaussian functions with arbitrary widths and peak heights. Visualization of the electronic orbitals and molecular structures was performed with the software program *Chemcraft* (http://www.chemcraftprog.com).

■ ASSOCIATED CONTENT

Supporting Information

The Supporting Information is available free of charge on the ACS Publications website at DOI: 10.1021/acs.inorgchem.7b01966.

Characterization data and mass, NMR, X-ray, absorption, and emission spectra for all of the compounds (PDF)

Accession Codes

CCDC 1564602 contains the supplementary crystallographic data for this paper. These data can be obtained free of charge via www.ccdc.cam.ac.uk/data_request/cif, or by emailing data_request@ccdc.cam.ac.uk, or by contacting The Cambridge Crystallographic Data Centre, 12 Union Road, Cambridge CB2 1EZ, UK; fax: +44 1223 336033.

■ AUTHOR INFORMATION

Corresponding Authors

*E-mail: lakshk@rpi.edu.
*E-mail: ravikanth@chem.iitb.ac.in.

ORCID

Vijayendra S. Shetti: 0000-0002-7656-5652
M. Ravikanth: 0000-0003-0193-6081

Author Contributions

‡A.A. and Y.P. contributed equally to this work.

Notes

The authors declare no competing financial interest.

■ ACKNOWLEDGMENTS

M.R. thanks the Science and Engineering Research Board, Government of India (Grant EMR/2015/002196), for financial support. A.A. thanks IIT Bombay for a research fellowship. The authors thank Dr. Uday R. Prabhu for helping with DOSY NMR spectroscopy. K.V.L. thanks the Center for Computational Innovations at Rensselaer Polytechnic Institute (Troy, NY) for computational time. We also thank Dr. Narahari Sastry and Dr. G. Gayatri, Indian Institute of Chemical Technology, Hyderabad, for their help in computational studies.

■ REFERENCES

(1) Suslick, K. S.; Rakow, N. A.; Kosal, M. E.; Chou, J.-H. The materials chemistry of porphyrins and metalloporphyrins. *J. Porphyrins Phthalocyanines* **2000**, *4*, 407−413.
(2) Burrell, A. K.; Officer, D. L.; Plieger, P. G.; Reid, D. C. W. Synthetic routes to multiporphyrin arrays. *Chem. Rev.* **2001**, *101*, 2751−2796.
(3) Shinokubo, H.; Osuka, A. Marriage of porphyrin chemistry with metal-catalysed reactions. *Chem. Commun.* **2009**, 1011−1021.
(4) Imamura, T.; Fukushima, K. Self-assembly of metallopyridylporphyrin oligomers. *Coord. Chem. Rev.* **2000**, *198*, 133−156.
(5) Wojaczyński, J.; Latos-Grażyński, L. Poly- and oligometalloporphyrins associated through coordination. *Coord. Chem. Rev.* **2000**, *204*, 113−171.
(6) Indelli, M. T.; Chiorboli, C.; Ghirotti, M.; Orlandi, M.; Scandola, F.; Kim, H. J.; Kim, H.-J. Photoinduced electron transfer in ruthenium(II)/tin(IV) multiporphyrin arrays. *J. Phys. Chem. B* **2010**, *114*, 14273−14282.
(7) Kiran, P. P.; Reddy, D. R.; Dharmadhikari, A. K.; Maiya, B. G.; Kumar, G. R.; Rao, D. N. Contribution of two-photon and excited state absorption in 'axial-bonding' type hybrid porphyrin arrays under resonant electronic excitation. *Chem. Phys. Lett.* **2006**, *418*, 442−447.
(8) Kiran, P. P.; Reddy, D. R.; Maiya, B. G.; Dharmadhikari, A. K.; Kumar, G. R.; Rao, D. N. Nonlinear absorption properties of 'axial-bonding' type tin(IV) tetratolylporphyrin based hybrid porphyrin arrays. *Opt. Commun.* **2005**, *252*, 150−161.
(9) Honda, T.; Nakanishi, T.; Ohkubo, K.; Kojima, T.; Fukuzumi, S. Formation of a long-lived photoinduced electron-transfer state in an electron acceptor-donor-acceptor porphyrin triad connected by coordination bonds. *J. Phys. Chem. C* **2010**, *114*, 14290−14299.
(10) Ou, Z.; E, W.; Zhu, W.; Thordarson, P.; Sintic, P. J.; Crossley, M. J.; Kadish, K. M. Effect of axial ligands and macrocyclic structure on redox potentials and electron-transfer mechanisms of Sn(IV) porphyrins. *Inorg. Chem.* **2007**, *46*, 10840−10849.
(11) Prodi, A.; Indelli, M. T.; Kleverlaan, C. J.; Alessio, E.; Scandola, F. Energy transfer pathways in pyridylporphyrin metal adducts and side-to-face arrays. *Coord. Chem. Rev.* **2002**, *229*, 51−58 and references cited therein.
(12) Scandola, F.; Chiorboli, C.; Prodi, A.; Iengo, E.; Alessio, E. Photophysical properties of metal-mediated assemblies of porphyrins. *Coord. Chem. Rev.* **2006**, *250*, 1471−1496 and references cited therein.
(13) Prodi, A.; Kleverlaan, C. J.; Indelli, M. T.; Scandola, F.; Alessio, E.; Iengo, E. Photophysics of pyridylporphyrin Ru(III) adducts: Heavy-atom effects and intramolecular decay pathways. *Inorg. Chem.* **2001**, *40*, 3498−3504.
(14) Prodi, A.; Indelli, M. T.; Kleverlaan, C. J.; Scandola, F.; Alessio, E.; Gianferrara, T.; Marzilli, L. G. Side-to-face ruthenium porphyrin arrays: Photophysical behaviour of dimeric and pentameric systems. *Chem. - Eur. J.* **1999**, *5*, 2668−2679.
(15) Iengo, E.; Zangrando, E.; Geremia, S.; Graff, R.; Kieffer, B.; Alessio, E. Two-point self-coordination of a dizinc(II) bispyridylporphyrin ruthenium complex leading selectively to a discrete molecular assembly: Solution and solid-state characterization. *Chem. - Eur. J.* **2002**, *8*, 4670−4674.
(16) Iengo, E.; Zangrando, E.; Alessio, E. Synthetic strategies and structural aspects of metal-mediated multiporphyrin assemblies. *Acc. Chem. Res.* **2006**, *39*, 841−851.
(17) Iengo, E.; Zangrando, E.; Alessio, E.; Chambron, J.-C.; Heitz, V.; Flamigni, L.; Sauvage, J.-P. A functionalized noncovalent macrocyclic multiporphyrin assembly from a dizinc(II) bis-porphyrin receptor and a free-base dipyridylporphyrin. *Chem. - Eur. J.* **2003**, *9*, 5879−5887.
(18) Drain, C. M.; Lehn, J.-M. Self-assembly of square multiporphyrin arrays by metal ion coordination. *J. Chem. Soc., Chem. Commun.* **1994**, 2313−2315.
(19) Hawley, J. C.; Bampos, N.; Sanders, J. K. M. Synthesis and characterization of carboxylate complexes of Sn^{IV} porphyrin monomers and oligomers. *Chem. - Eur. J.* **2003**, *9*, 5211−5222.

DOI: 10.1021/acs.inorgchem.7b01966
Inorg. Chem. XXXX, XXX, XXX−XXX

(20) Iengo, E.; Zangrando, E.; Alessio, E. Discrete supramolecular assemblies of porphyrins mediated by coordination compounds. *Eur. J. Inorg. Chem.* **2003**, *2003*, 2371−2384.
(21) Satake, A.; Kobuke, Y. Dynamic supramolecular porphyrin systems. *Tetrahedron* **2005**, *61*, 13−41.
(22) Beletskaya, I.; Tyurin, V. S.; Tsivadze, A. Y.; Guilard, R.; Stern, C. Supramolecular chemistry of metalloporphyrins. *Chem. Rev.* **2009**, *109*, 1659−1713.
(23) Redman, J. E.; Feeder, N.; Teat, S. J.; Sanders, J. K. M. Rh(III) porphyrins as building blocks for porphyrin coordination arrays: From dimers to heterometallic undecamers. *Inorg. Chem.* **2001**, *40*, 2486−2499.
(24) Fallon, G. D.; Langford, S. J.; Lee, M. A.-P.; Lygris, E. Self-assembling mixed porphyrin trimers- the use of diaxial Sn(IV) porphyrin phenolates as an organising precept. *Inorg. Chem. Commun.* **2002**, *5*, 715−718.
(25) Maiya, B. G.; Bampos, N.; Asok Kumar, A.; Feeder, N.; Sanders, J. K. M. A supramolecular array assembled via the complementary binding properties of ruthenium(II) and tin(IV) porphyrins. *New J. Chem.* **2001**, *25*, 797−800.
(26) Shetti, V. S.; Ravikanth, M. Supramolecular tetrads containing Sn(IV) porphyrin, Ru(II) porphyrin, and expanded porphyrins assembled using complementary metal-ligand interactions. *Inorg. Chem.* **2011**, *50*, 1713−1722.
(27) Dvivedi, A.; Pareek, Y.; Ravikanth, M. Sn^{IV} porphyrin scaffolds for axially bonded multiporphyrin arrays: Synthesis and structure elucidation by NMR studies. *Chem. - Eur. J.* **2014**, *20*, 4481−4490.
(28) Lee, S. J.; Hupp, J. T. Porphyrin-containing molecular squares: Design and applications. *Coord. Chem. Rev.* **2006**, *250*, 1710−1723 and references cited therein.
(29) Alessio, E.; Geremia, S.; Mestroni, S.; Iengo, E.; Srnova, I.; Slouf, M. Solution and solid state structure of a canted, side-to-face, bis(porphyrin) adduct. *Inorg. Chem.* **1999**, *38*, 869−875.
(30) Kumar, A. A.; Giribabu, L.; Reddy, D. R.; Maiya, B. G. New molecular arrays based on a tin(IV) porphyrin scaffold. *Inorg. Chem.* **2001**, *40*, 6757−6766.
(31) Giribabu, L.; Rao, T. A.; Maiya, B. G. "Axial-bonding"-type hybrid porphyrin arrays: Synthesis, spectroscopy, electrochemistry, and singlet state properties. *Inorg. Chem.* **1999**, *38*, 4971−4980.
(32) Pareek, Y.; Lakshmi, V.; Ravikanth, M. Axially bonded pentads constructed on the Sn(IV) porphyrin scaffold. *Dalton Trans.* **2014**, *43*, 6870−6879.
(33) Shetti, V. S.; Ravikanth, M. Sn(IV) porphyrin based axial-bonding type porphyrin triads containing heteroporphyrins as axial ligands. *Inorg. Chem.* **2010**, *49*, 2692−2700.
(34) Tong, Y.; Hamilton, D. G.; Meillon, J.-C.; Sanders, J. K. M. Sn(IV) porphyrins as NMR shift reagents and supramolecular protecting groups: preparation of a carboxylate-catenane porphyrin complex. *Org. Lett.* **1999**, *1*, 1343−1346.
(35) Webb, S. J.; Sanders, J. K. M. A tin(IV)-ruthenium(II)-tin(IV) cyclic porphyrin trimer with replaceable chiral linings. *Inorg. Chem.* **2000**, *39*, 5920−5929.
(36) Crossley, M. J.; Thordarson, P.; Wu, R. A.-S. Efficient formation of lipophilic dihydroxotin(IV) porphyrins and bis-porphyrins. *J. Chem. Soc., Perkin Trans. 1* **2001**, 2294−2302.
(37) Langford, S. J.; Lau, V.-L.; Lee, M. A.-P.; Lygris, E. Porphyrin-based supermolecules and supramolecular arrays. *J. Porphyrins Phthalocyanines* **2002**, *6*, 748−756.
(38) Fallon, G. D.; Lee, M. A.-P.; Langford, S. J.; Nichols, P. J. Metalloporphyrin molecular sieves based on tin(IV) porphyrin phenolates. *Org. Lett.* **2002**, *4*, 1895−1898.
(39) Ou, Z.; E, W.; Zhu, W.; Thordarson, P.; Sintic, P. J.; Crossley, M. J.; Kadish, K. M. Effect of axial ligands and macrocyclic structure on redox potentials and electron-transfer mechanisms of Sn(IV) porphyrins. *Inorg. Chem.* **2007**, *46*, 10840−10849.
(40) Giribabu, L.; Kumar, C. V.; Reddy, P. Y. Axial-bonding heterotrimers based on tetrapyrrolic rings: synthesis, characterization, and redox and photophysical properties. *Chem. - Asian J.* **2007**, *2*, 1574−1580.
(41) Lee, S. J.; Jensen, R. A.; Malliakas, C. D.; Kanatzidis, M. G.; Hupp, J. T.; Nguyen, S. T. Effect of secondary substituent on the physical properties, crystal structures, and nanoparticles morphologies of (porphyrin)$Sn(OH)_2$: diversity enabled *via* synthetic manipulations. *J. Mater. Chem.* **2008**, *18*, 3640−3642.
(42) Arnold, D. P.; Blok, J. The coordination chemistry of tin porphyrin complexes. *Coord. Chem. Rev.* **2004**, *248*, 299−319 and references cited therein.
(43) Shetti, V. S.; Pareek, Y.; Ravikanth, M. Sn(IV) porphyrin scaffold for multiporphyrin arrays. *Coord. Chem. Rev.* **2012**, *256*, 2816−2842.
(44) Kim, H.-J.; Bampos, N.; Sanders, J. K. M. Assembly of dynamic heterometallic oligoporphyrins using cooperative zinc-nitrogen, ruthenium-nitrogen, and tin-oxygen coordination. *J. Am. Chem. Soc.* **1999**, *121*, 8120−8121.
(45) Fallon, G. D.; Langford, S. J.; Lee, M. A.-P.; Lygris, E. Self-assembling mixed porphyrin trimers- the use of diaxial Sn(IV)-porphyrin phenolates as an organising precept. *Inorg. Chem. Commun.* **2002**, *5*, 715−718.
(46) Langford, S. J.; Woodward, C. P. Six-sided heptaporphyrin array: Towards a nano-sized cube. *Collect. Czech. Chem. Commun.* **2004**, *69*, 996−1008.
(47) Hunter, C. A.; Tomas, S. Accurate length control of supramolecular oligomerization: Vernier assemblies. *J. Am. Chem. Soc.* **2006**, *128*, 8975−8979.
(48) Metselaar, G. A.; Ballester, P.; de Mendoza, J. Cyclic oligomers based on complementary Zn(II) and Sn(IV)-porphyrins. *New J. Chem.* **2009**, *33*, 777−783.
(49) Shetti, V. S.; Ravikanth, M. A simple alternative method for preparing Sn(IV) porphyrins. *J. Porphyrins Phthalocyanines* **2010**, *14*, 361−370.
(50) Frisch, M. J.; Trucks, G. W.; Schlegel, H. B.; Scuseria, G. E.; Robb, M. A.; Cheeseman, J. R.; Scalmani, G.; Barone, V.; Mennucci, B.; Petersson, G. A.; Nakatsuji, H.; Caricato, M.; Li, X.; Hratchian, H. P.; Izmaylov, A. F.; Bloino, J.; Zheng, G.; Sonnenberg, J. L.; Hada, M.; Ehara, M.; Toyota, K.; Fukuda, R.; Hasegawa, J.; Ishida, M.; Nakajima, T.; Honda, Y.; Kitao, O.; Nakai, H.; Vreven, T.; Montgomery, J. A., Jr; Peralta, J. E.; Ogliaro, F.; Bearpark, M.; Heyd, J. J.; Brothers, E.; Kudin, K. N.; Staroverov, V. N.; Kobayashi, R.; Normand, J.; Raghavachari, K.; Rendell, A.; Burant, J. C.; Iyengar, S. S.; Tomasi, J.; Cossi, M.; Rega, N.; Millam, J. M.; Klene, M.; Knox, J. E.; Cross, J. B.; Bakken, V.; Adamo, C.; Jaramillo, J.; Gomperts, R.; Stratmann, R. E.; Yazyev, O.; Austin, A. J.; Cammi, R.; Pomelli, C.; Ochterski, J. W.; Martin, R. L.; Morokuma, K.; Zakrzewski, V. G.; Voth, G. A.; Salvador, P.; Dannenberg, J. J.; Dapprich, S.; Daniels, A. D.; Farkas, Ö.; Foresman, J. B.; Ortiz, J. V.; Cioslowski, J.; Fox, D. J. *Gaussian 09*, revision A.02; Gaussian, Inc.: Wallingford, CT, 2009.
(51) (a) Dey, S.; Mondal, P.; Rath, S. P. Aggregation-controlled excimer emission in an axial anthracene-Sn(IV)porphyrin-anthracene triad in the solid and solution phases. *New J. Chem.* **2015**, *39*, 4100−4108. (b) Maeda, D.; Shimakoshi, H.; Abe, M.; Fujitsuka, M.; Majima, T.; Hisaeda, Y. Synthesis of a novel Sn(IV) porphycene-ferrocene triad linked by axial coordination and solvent polarity effect in photo-induced charge separation process. *Inorg. Chem.* **2010**, *49*, 2872−2880. (c) Redman, J. E.; Feeder, N.; Teat, S. J.; Sanders, J. K. M. Rh(III) porphyrins as building blocks for porphyrin coordination arrays: From dimers to heterometallic undecamers. *Inorg. Chem.* **2001**, *40*, 2486−2499. (d) Guenet, A.; Graf, E.; Kyritsakas, N.; Hosseini, M. W. Design and synthesis of Sn-porphyrin based molecular gates. *Inorg. Chem.* **2010**, *49*, 1872−1883.
(52) Latos- Grażyński, L.; Lisowski, J.; Olmstead, M. M.; Balch, A. L. 21-Thiatetra-*p*-tolylporphyrin and its copper(II) bicarbonate complex. Structural effects of copper-thiophene binding. *J. Am. Chem. Soc.* **1987**, *109*, 4428−4429.
(53) Latos-Grażyński, L.; Lisowski, J.; Szterenberg, S.; Olmstead, M. M.; Balch, A. L. Crystal and molecular structure of 21-Thia-5,20-diphenyl-10,15-bis(*p*-nitrophenyl)-porphyrin and 21,23-Dithiatetraphenylporphyrin. The influence of sulfur on the π-delocalization pattern. *J. Org. Chem.* **1991**, *56*, 4043−4045.

DOI: 10.1021/acs.inorgchem.7b01966
Inorg. Chem. XXXX, XXX, XXX−XXX

(54) Gebauer, A.; Schmidt, J. A. R.; Arnold, J. Synthesis, characterization, and properties of a lithium 21-Thiaporphyrin complex. *Inorg. Chem.* **2000**, *39*, 3424−3427.
(55) Zhu, Y.; Zhu, Y.-Z.; Song, H.-B.; Zheng, J.-Y.; Liu, Z.-B.; Tian, J.-G. Synthesis and crystal structure of 21,23-dithiaporphyrins and their nonlinear optical activities. *Tetrahedron Lett.* **2007**, *48*, 5687−5691.
(56) Solntsev, P. V.; Sabin, J. R.; Dammer, S. J.; Gerasimchuk, N. N.; Nemykin, V. N. Unexpected fluorescence properties in an axially σ-bonded ferrocenyl-containing porphyrin. *Chem. Commun.* **2010**, *46*, 6581−6583.
(57) Langford, S. J.; Woodward, C. P. Supramolecular self-assembly of dihydroxy tin(IV) porphyrin stabilized helical water chains. *CrystEngComm* **2007**, *9*, 218−221.
(58) Wang, S.; Forsyth, C.; Langford, S. J. Supramolecular materials with robust and tunable channels constructed from tin(IV)porphyrin phenolates. *CrystEngComm* **2015**, *17*, 3060−3063.
(59) Soujanya, Y.; Punnagai, M.; Sateesh, B.; Sastry, G. N. DFT study of core-modified porphyrin isomers. *Int. J. Quantum Chem.* **2007**, *107*, 134−151.
(60) Bromby, A. D.; Jansonius, R. P.; Sutherland, T. C. Synthesis and optical and electronic properties of core-modified 21,23-dithiaporphyrins. *J. Org. Chem.* **2013**, *78*, 1612−1620.
(61) Szterenberg, L.; Sprutta, N.; Latos-Grażyński, L. Thiaporphyrin with an inverted thiophene ring- DFT studies. *J. Inclusion Phenom. Mol. Recognit. Chem.* **2001**, *41*, 209−213.
(62) Agnihotri, N.; Steer, R. P. DFT and TD-DFT calculations of axially substituted tin porphyrins and an ethynyl-linked tin porphyrin dimer. *J. Porphyrins Phthalocyanines* **2015**, *19*, 610−621.
(63) Girichev, G. V.; Giricheva, N. I.; Koifman, O. I.; Minenkov, Y. V.; Pogonin, A. E.; Semeikin, A. S.; Shlykov, S. A. Molecular structure and bonding in octamethylporphyrin tin(II), $SnN_4C_{28}H_{28}$. *Dalton Trans.* **2012**, *41*, 7550−7558.
(64) Sheldrick, G. M. *Program for Crystal Structure Solution and Refinement*; University of Goettingen: Goettingen, Germany, 1997 (*Acta Crystallogr., Sect. A* **2008**, *A64*, 112).
(65) Kresse, G.; Furthmüller, J. Efficient iterative schemes for *ab initio* total-energy calculations using a palne-wave basis set. *Phys. Rev. B: Condens. Matter Mater. Phys.* **1996**, *54*, 11169−11186.
(66) Perdew, J. P.; Burke, K.; Ernzerhof, M. Generalized gradient approximation made simple. *Phys. Rev. Lett.* **1996**, *77*, 3865−3868.
(67) Kresse, G.; Joubert, D. From ultrasoft pseudopotentials to the projector augmented-wave method. *Phys. Rev. B: Condens. Matter Mater. Phys.* **1999**, *59*, 1758−1775.
(68) Grimme, S. Semiempirical GGA-type density functional constructed with a long-range dispersion correction. *J. Comput. Chem.* **2006**, *27*, 1787−1799.
(69) Hanwell, M. D.; Curtis, D. E.; Lonie, D. C.; Vandermeersch, T.; Zurek, E.; Hutchison, G. R. Avogadro: an advanced semantic chemical editor, visualization, and analysis platform. *J. Cheminf.* **2012**, *4*, 17.
(70) Becke, A. D. Density-functional thermochemistry. III. The role of exact exchange. *J. Chem. Phys.* **1993**, *98*, 5648−5652.
(71) Izsák, R.; Neese, F. An overlap fitted chain of spheres exchange method. *J. Chem. Phys.* **2011**, *135*, 144105.
(72) Kossmann, S.; Neese, F. Comparison of two efficient approximate Hartree-Fock approaches. *Chem. Phys. Lett.* **2009**, *481*, 240−243.
(73) Neese, F.; Wennmohs, F.; Hansen, A.; Becker, U. Efficient, approximate and parallel Hartree-Fock and hybrid DFT calculations. A 'chain-of-spheres' algorithm for the Hartree-Fock exchange. *Chem. Phys.* **2009**, *356*, 98−109.
(74) Neese, F. An improvement of the resolution of the identity approximation for the formation of the coulomb matrix. *J. Comput. Chem.* **2003**, *24*, 1740−1747.
(75) Neese, F. The ORCA program system. *Comput. Mol. Sci.* **2012**, *2*, 73−78.
(76) Neese, F. Approximate second-order SCF convergence for spin unrestricted wavefunctions. *Chem. Phys. Lett.* **2000**, *325*, 93−98.
(77) Valeev, E. F. *LIBINT: A library for the evaluation of molecular integrals of many-body operators over Gaussian functions*, version 2.1.0 (beta), http://libint.valeyev.net/.
(78) Hay, P. J.; Wadt, W. R. *Ab initio* effective core potentials for molecular calculations. Potentials for the transition metal atoms Sc to Hg. *J. Chem. Phys.* **1985**, *82*, 270−283.
(79) Wadt, W. R.; Hay, P. J. *Ab initio* effective core potentials for molecular calculations. Potentials for main group elements Na to Bi. *J. Chem. Phys.* **1985**, *82*, 284−298.
(80) Hay, P. J.; Wadt, W. R. *Ab initio* effective core potentials for molecular calculations. Potentials for K to Au including the outermost core orbitals. *J. Chem. Phys.* **1985**, *82*, 299−310.
(81) Weigend, F. Accurate coulomb-fitting basis sets for H to Rn. *Phys. Chem. Chem. Phys.* **2006**, *8*, 1057−1065.
(82) Barone, V.; Cossi, M. Quantum calculation of molecular energies and energy gradients in solution by a conductor solvent model. *J. Phys. Chem. A* **1998**, *102*, 1995−2001.
(83) Petrenko, T.; Kossmann, S.; Neese, F. Efficient time-dependent density functional theory approximations for hybrid density functionals: Analytical gradients and parallelization. *J. Chem. Phys.* **2011**, *134*, 054116.
(84) Petrenko, T.; Krylova, O.; Neese, F.; Sokolowski, M. Optical absorption and emission properties of rubrene: insight from a combined experimental and theoretical study. *New J. Phys.* **2009**, *11*, 015001.
(85) Grimme, S.; Neese, F. Double-hybrid density functional theory for excited electronic states of molecules. *J. Chem. Phys.* **2007**, *127*, 154116.
(86) Neese, F.; Olbrich, G. Efficient use of the resolution of the identity approximation in time-dependent density functional calculations with hybrid density functionals. *Chem. Phys. Lett.* **2002**, *362*, 170−178.

DOI: 10.1021/acs.inorgchem.7b01966
Inorg. Chem. XXXX, XXX, XXX−XXX